



Measurement of forward J/ψ production cross-sections in pp collisions at $\sqrt{s} = 13$ TeV

The LHCb collaboration[†]

Abstract

The production of J/ψ mesons in proton-proton collisions at a centre-of-mass energy of $\sqrt{s} = 13$ TeV is studied with the LHCb detector. Cross-section measurements are performed as a function of the transverse momentum p_T and the rapidity y of the J/ψ meson in the region $p_T < 14$ GeV/ c and $2.0 < y < 4.5$, for both prompt J/ψ mesons and J/ψ mesons from b -hadron decays. The production cross-sections integrated over the kinematic coverage are $15.30 \pm 0.03 \pm 0.86$ μb for prompt J/ψ and $2.34 \pm 0.01 \pm 0.13$ μb for J/ψ from b -hadron decays, assuming zero polarization of the J/ψ meson. The first uncertainties are statistical and the second systematic. The cross-section reported for J/ψ mesons from b -hadron decays is used to extrapolate to a total $b\bar{b}$ cross-section. The ratios of the cross-sections with respect to $\sqrt{s} = 8$ TeV are also determined.

Submitted to JHEP

© CERN on behalf of the LHCb collaboration, licence CC-BY-4.0.

[†]Authors are listed at the end of this paper.

1 Introduction

The study of heavy quarkonium production in pp collisions provides important information on both the perturbative and the non-perturbative regimes of quantum chromodynamics (QCD). Heavy quarkonium production can be described in two stages. The first is the short-distance production of a heavy quark pair, $Q\bar{Q}$, which can be described perturbatively and the second is the non-perturbative hadronisation of the heavy quark pair into quarkonium state, such as the J/ψ meson. The non-perturbative part cannot yet be determined reliably, and must be determined using experimental results. After almost forty years of theoretical and experimental efforts, the hadronic production of quarkonia is still not fully understood. In the colour singlet model (CSM) [1–7], the intermediate $Q\bar{Q}$ state is assumed to be colourless, and has the same J^{PC} quantum numbers as the final-state quarkonium. In the non-relativistic QCD (NRQCD) approach [8–10], all viable colour and spin-parity quantum numbers are allowed for the intermediate $Q\bar{Q}$ state, and each configuration is assigned a probability to transform into the specific quarkonium state. The transition probabilities are described by universal long-distance matrix elements (LDME) determined from experimental data.

In pp collisions, J/ψ mesons can be produced directly from hard collisions of partons, through the feed-down of excited charmonium states, or via decays of b -flavoured hadrons. The first two sources are collectively referred to as prompt J/ψ production, while the third process is referred to in the following as “ J/ψ -from- b ”.

The J/ψ differential production cross-section has been measured with LHC data in pp collisions at centre-of-mass energies of 2.76 TeV [11, 12], 7 TeV [13–17], and 8 TeV [18]. Next-to-leading order CSM calculations [19, 20] give a better description of the experimental data than leading order (LO) calculations at high J/ψ transverse momentum ($p_{\text{T}}/c > M(J/\psi)$). However, CSM calculations still underestimate the prompt J/ψ production cross-section. On the other hand, NRQCD calculations with LDME determined from CDF data [21] describe well the p_{T} dependence of the prompt J/ψ cross-section at both the Tevatron [22, 23] and the LHC experiments [24–26]. The measured J/ψ -from- b production cross-section and its dependence on p_{T} at the LHC are in good agreement with predictions from fixed order plus next-to-leading logarithms (FONLL) [27] calculations.

The J/ψ polarisation was measured by the ALICE [28], CMS [29] and LHCb [30] collaborations in pp collisions at $\sqrt{s} = 7$ TeV. The measurements by ALICE were performed for inclusive J/ψ meson production, while CMS and LHCb disentangled prompt J/ψ and J/ψ -from- b mesons. Next-to-leading order CSM calculations predict a large longitudinal polarisation of the J/ψ meson [31], while NRQCD calculations predict a large J/ψ transverse polarisation at high p_{T} [32–35]. Neither prediction is supported by experimental results [28–30, 36–39].

This paper reports J/ψ cross-section measurements in pp collisions at $\sqrt{s} = 13$ TeV in the J/ψ kinematic range $p_{\text{T}} < 14$ GeV/ c and $2.0 < y < 4.5$, using J/ψ decaying to $\mu^+\mu^-$ final states. Under the assumption of zero J/ψ polarisation (see Sec. 5 for detailed discussion), the following quantities are measured: the double differential cross-sections as a function of p_{T} and y ; the integrated production cross-sections for prompt J/ψ and

J/ψ -from- b ; the $b\bar{b}$ production cross-section; and the ratio of cross-sections with respect to the J/ψ cross-sections in pp collisions at $\sqrt{s} = 8$ TeV previously measured by LHCb [18].

2 The LHCb detector and data set

The data used in this analysis come from pp collisions at $\sqrt{s} = 13$ TeV, collected by the LHCb detector in July 2015, with an average of 1.1 visible interactions per bunch crossing and correspond to an integrated luminosity of $3.05 \pm 0.12 \text{ pb}^{-1}$. The LHCb detector [40, 41] is a single-arm forward spectrometer covering the pseudorapidity range $2 < \eta < 5$, designed for the study of particles containing b or c quarks. The detector includes a high-precision tracking system consisting of a silicon-strip vertex detector surrounding the pp interaction region, a large-area silicon-strip detector located upstream of a dipole magnet with a bending power of about 4 Tm, and three stations of silicon-strip detectors and straw drift tubes placed downstream of the magnet. The tracking system provides a measurement of momentum, p , of charged particles with a relative uncertainty that varies from 0.5% at low momentum to 1.0% at 200 GeV/ c . Different types of charged hadrons are distinguished using information from two ring-imaging Cherenkov detectors. Photons, electrons and hadrons are identified by a calorimeter system consisting of scintillating-pad and preshower detectors, an electromagnetic calorimeter and a hadronic calorimeter. Muons are identified by a system composed of alternating layers of iron and multiwire proportional chambers [42].

The online event selection consists of a hardware stage, based on information from the calorimeter and muon systems, followed by a software stage, which performs J/ψ candidate reconstruction. The hardware trigger selects events with at least one muon candidate with transverse momentum $p_T > 0.9 \text{ GeV}/c$. In the first stage of the software trigger, two muon tracks with $p_T > 500 \text{ MeV}/c$ are required to form a J/ψ candidate with invariant mass $M(\mu^+\mu^-) > 2.7 \text{ GeV}/c^2$. In the second stage, J/ψ candidates with good vertex fit quality and invariant mass within $150 \text{ MeV}/c^2$ of the known value [43] are selected.

This analysis benefits from a new scheme for the LHCb software trigger introduced for LHC Run 2. Alignment and calibration is performed in near real-time [44] and updated constants are made available for the trigger. The same alignment and calibration information is propagated to the offline reconstruction, to ensure consistent and high-quality particle identification information for the trigger and offline. The larger timing budget available in the trigger with respect to LHC Run 1 also results in the convergence of the online and offline track reconstruction, such that offline performance is achieved in the trigger. The identical performance of the online and offline reconstruction achieved in this way offers the opportunity to perform physics analyses directly using candidates reconstructed in the trigger [45]. The storage of only the triggered candidates enables a reduction in the event size by an order of magnitude. The analysis described in this paper uses the online reconstruction for the first time in LHCb, and is checked against the standard offline reconstruction chain.

Simulated samples are used to evaluate the J/ψ detection efficiency. In the simulation,

pp collisions are generated using PYTHIA 6 [46] with a specific LHCb configuration [47]. Decays of hadronic particles are described by EVTGEN [48], in which final-state radiation is generated using PHOTOS [49]. The prompt charmonium production is simulated in PYTHIA with contributions from both the leading order colour-singlet and colour-octet contributions [47, 50], and the charmonium is generated unpolarised. The interaction of the generated particles with the detector, and its response, are simulated using the GEANT4 toolkit [51] as described in Ref. [52].

3 Selection of J/ψ candidates

The J/ψ candidates are selected in the second step of the software trigger. Each event is required to have at least one primary vertex (PV) reconstructed from at least four tracks found by the vertex detector. For events with multiple PVs, the PV which has the smallest χ_{IP}^2 with respect to the J/ψ candidate is chosen. The χ_{IP}^2 is defined as the change of the primary vertex fit quality when the J/ψ meson is excluded from the PV fit. Each identified muon track is required to have $p_{\text{T}} > 0.7 \text{ GeV}/c$, $p > 3 \text{ GeV}/c$, and to have a good quality track fit. The muon tracks of the J/ψ candidate must form a good quality two-track vertex. Duplicate tracks created by the reconstruction are suppressed to the level of 0.5×10^{-3} .

The reconstructed vertex of the J/ψ mesons originating from b -hadron decays tends to be separated from the PVs, and thus these can be distinguished from prompt J/ψ mesons by exploiting the pseudo decay time defined as

$$t_z = \frac{(z_{J/\psi} - z_{\text{PV}}) \times M_{J/\psi}}{p_z}, \quad (1)$$

where $z_{J/\psi} - z_{\text{PV}}$ is the distance along the beam axis between the J/ψ decay vertex and the PV, p_z is the z -component of the J/ψ momentum, and $M_{J/\psi}$ the known J/ψ mass [43].

The J/ψ candidates with $|t_z| < 10 \text{ ps}$, corresponding to less than 7 times the b -hadron lifetime, are selected for the fits to the t_z distribution. To further select good J/ψ candidates, the uncertainty on t_z , which is propagated from the uncertainties provided by the track reconstruction, is required to be less than 0.3 ps.

4 Cross-section determination

The double differential J/ψ production cross-section in each kinematic bin of p_{T} and y is defined as

$$\frac{d^2\sigma}{dydp_{\text{T}}} = \frac{N(J/\psi \rightarrow \mu^+\mu^-)}{L_{\text{int}} \times \varepsilon_{\text{tot}} \times \mathcal{B}(J/\psi \rightarrow \mu^+\mu^-) \times \Delta y \times \Delta p_{\text{T}}}, \quad (2)$$

where $N(J/\psi \rightarrow \mu^+\mu^-)$ is the yield of prompt J/ψ or J/ψ -from- b signal mesons, ε_{tot} is the total detection efficiency in the given kinematic bin, L_{int} is the integrated luminosity, $\mathcal{B}(J/\psi \rightarrow \mu^+\mu^-) = (5.961 \pm 0.033)\%$ [43] is the branching ratio of the decay $J/\psi \rightarrow \mu^+\mu^-$

and $\Delta p_T = 1 \text{ GeV}/c$ and $\Delta y = 0.5$ are the bin widths. The measurements are restricted to $p_T < 14 \text{ GeV}/c$ due to limited data at higher transverse momenta.

The absolute luminosity is determined from the beam profiles and beam currents. The beam profiles and their overlap integral are measured using a beam-gas imaging method [53, 54], where neon is injected into the beam vacuum around the interaction point. The beam currents are measured by LHC instruments, which determine the bunch population fractions and the total beam intensity. Furthermore, information on beam-gas interactions not originating from nominally filled bunch slots is used to determine the charge fraction not participating in bunch collisions. The integrated luminosity for this analysis is calibrated using the number of visible pp interactions measured during the beam-gas imaging runs and during the runs used for this analysis. From this procedure, the integrated luminosity is measured to be $3.05 \pm 0.12 \text{ pb}^{-1}$.

The efficiency ε_{tot} is determined as the product of the reconstruction and selection efficiencies, muon identification efficiency and trigger efficiency, and is calculated using simulated samples in each (p_T, y) bin, independently for prompt J/ψ and J/ψ -from- b . The track reconstruction and the muon identification efficiency are corrected using data-driven techniques, while the trigger efficiencies are also validated using data, as explained in Sec. 5.

The yield of J/ψ signal events, both from prompt J/ψ and J/ψ -from- b , is determined from a two-dimensional unbinned maximum likelihood fit to the invariant mass and pseudo decay time of the candidates, performed independently for each (p_T, y) bin. The invariant mass distribution of the signal is described by the sum of two Crystal Ball (CB) functions [55] with a common mean value and different widths. The parameters of the power law tails, the relative fractions and the difference between the widths of the two CB functions are fixed to values obtained from the simulation, leaving the mean and one width of the CB function as free parameters. The combinatorial background is described by an exponential distribution.

The fraction of J/ψ -from- b candidates, F_b , is determined from the fit to the t_z distribution. The t_z distribution of prompt J/ψ is described by a Dirac δ function at $t_z = 0$, and that of J/ψ -from- b by an exponential decay function, which are both convolved with a double-Gaussian resolution function. A J/ψ candidate can also be associated to a wrong PV, resulting in a long tail component in the t_z distribution. The fraction of the tail is below 0.5% of all events. Its shape is modelled from data by calculating t_z with the J/ψ candidate from a given event and the closest PV in the next event of the sample. The background t_z distribution is parametrised with an empirical function based on the observed shape of the t_z distribution in the J/ψ mass sidebands. The background comes from muons of semileptonic b - and c -hadron decays and from pions and kaons decaying in-flight. It is parametrised as the sum of a Dirac δ function and five exponential functions, three for positive t_z and two for negative t_z . The function is convolved with a double-Gaussian resolution function similar to that used for the signal, but with different parameters. All parameters of the background t_z distribution are fixed to values determined from the J/ψ mass sidebands independently in each (p_T, y) bin.

The total J/ψ signal yield determined from the fit is about one million events. An

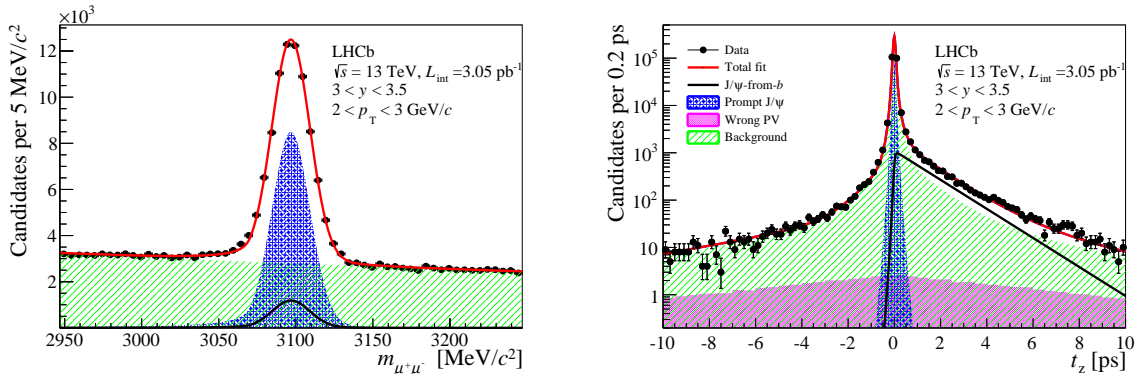


Figure 1: Invariant mass (left) and pseudo decay time (right) distributions for the kinematic bin $2 < p_T < 3 \text{ GeV}/c$, $3.0 < y < 3.5$, with fit results superimposed. The solid (red) line is the total fit function, the shaded (green) area corresponds to the background component. The prompt J/ψ contribution is shown in cross-hatched area (blue), J/ψ -from- b in a solid (black) line and the tail contribution due to the association of J/ψ with the wrong PV is shown in full filled (magenta) area. The tail contribution is not visible in the invariant mass plot.

example for one (p_T, y) bin of the invariant mass and the pseudo decay time distributions is shown in Fig. 1 with the one-dimensional projections of the fit result superimposed.

5 Systematic uncertainties

Systematic uncertainties, most of which apply to both prompt J/ψ and J/ψ -from- b mesons, are summarised in Table 1 and described below.

The uncertainty related to the modelling of the signal mass shape is studied by replacing the nominal model with a Hypatia function [56], which takes into account the mass uncertainty distribution. The relative difference of the signal yield is about 1.0%, which is taken as a fully correlated systematic uncertainty in each bin.

Due to the presence of bremsstrahlung in the $J/\psi \rightarrow \mu^+\mu^-$ decay, a fraction of J/ψ events fall outside the mass window used in this analysis. The efficiency of the mass window selection is determined from simulation, and based on a detailed comparison between the radiative tails in simulation and data, a value of 1.0% of the yield is assigned as the systematic uncertainty.

To calibrate the muon identification efficiency determined from simulation, the single-track muon identification efficiency is measured with a $J/\psi \rightarrow \mu^+\mu^-$ data sample using a tag-and-probe method. In this method, the J/ψ candidates are reconstructed with only one track identified as a muon (“tag”). The single muon identification efficiency is measured as the probability of the other track (“probe”) to be identified as a muon, in bins of momentum, p_μ , and pseudorapidity, η_μ of the probe track. The single-track muon identification efficiency obtained in data is weighted with the (p_μ, η_μ) distribution of the muons from J/ψ mesons in simulation. The resulting efficiency is divided by that

determined directly from simulation, giving 1.050 ± 0.017 , which is used to correct the muon identification efficiency in each (p_T, y) bin of the J/ψ meson. The uncertainty on the correction factor, limited by the calibration sample size in data, is used to obtain the systematic uncertainty. The choice of binning scheme in (p_μ, η_μ) is another source of systematic uncertainty and is evaluated by choosing alternative binning schemes. In total the systematic uncertainty on the cross-sections due to the muon identification is 1.8%.

The tracking efficiency is studied with a data-driven tag-and-probe approach with J/ψ decays using partially reconstructed tracks, where one muon track is fully reconstructed as the tag track, and the probe track is reconstructed using only specific sub-detectors [57]. The simulated sample is weighted to agree in event multiplicity with the data sample. A systematic uncertainty of the efficiency of 0.4% per muon track is assigned to account for a different event multiplicity between data and simulation. The tracking efficiency is determined to be the fraction of $J/\psi \rightarrow \mu^+\mu^-$ decays where the probe track can be matched to a fully reconstructed track. The ratio of the resulting tracking efficiency between data and simulation is used to weight the simulation sample according to pseudorapidity and momentum of muons to obtain an efficiency correction in each (p_T, y) bin of the J/ψ meson. In total the correction factor ranges from 0.94 to 1.04, depending on the J/ψ (p_T, y) bin. The uncertainty on the muon track efficiency correction factor is limited by the size of the calibration data sample, and is propagated into the systematic uncertainty on the cross-section measurements. In total, the systematic uncertainty on the cross-sections related to the tracking efficiency is in the range of 1 – 3%, depending on the J/ψ (p_T, y) bin.

The J/ψ vertex fit quality requirement leads to an uncertainty of 0.4% for the selection

Table 1: Relative systematic uncertainties (in %) on the J/ψ cross-section measurements. The uncertainty from the t_z fit only affects J/ψ -from- b mesons. Most of the uncertainties are fully correlated between bins, with the exception of the p_T, y spectrum dependence and the simulation statistics, which are considered uncorrelated.

Source	Systematic uncertainty (%)
Luminosity	3.9
Hardware trigger	0.1 – 5.9
Software trigger	1.5
Muon ID	1.8
Tracking	1.1 – 3.4
Radiative tail	1.0
J/ψ vertex fit	0.4
Signal mass shape	1.0
$\mathcal{B}(J/\psi \rightarrow \mu^+\mu^-)$	0.6
p_T, y spectrum	0.1 – 5.0
Simulation statistics	0.3 – 5.0
t_z fit (J/ψ -from- b only)	0.1

efficiency, which is determined by comparing the distributions of the vertex fit quality between data and simulation.

The trigger efficiency obtained from simulation is cross-checked using data-driven methods using a fully reconstructed J/ψ sample. For the hardware trigger, a tag-and-probe method is used to evaluate the single track muon trigger efficiency in bins of muon transverse momentum, $p_{T\mu}$, and pseudorapidity, η_μ , for both simulation and data. In this procedure, the J/ψ candidate is required to pass both steps of the software trigger. The J/ψ trigger efficiency is calculated by weighting $p_{T\mu}$ and η_μ of the muons with the single-muon track trigger efficiency obtained from data and simulation, and their relative difference is quoted as a systematic uncertainty. For most of the J/ψ (p_T, y) bins, the systematic effect on the cross-section is found to be below 1.0%, but in two bins an uncertainty of 5.9% is found. The software trigger efficiency is determined using a subset of events that would have triggered if the J/ψ signals were excluded [45]. The efficiency is computed in each (p_T, y) bin for data and simulation, and the relative difference between data and simulation of about 1.5% is taken as a systematic uncertainty.

The possible discrepancy between the p_T and y distributions of J/ψ mesons in data and simulation for each bin is studied by reweighting the distribution in simulation to that in data. The relative difference between the efficiency after reweighting and the nominal efficiency is taken as a systematic uncertainty and found to be in the range 0.1% – 5%, depending on the (p_T, y) bin of the J/ψ meson, where the largest value corresponds to the bins at the LHCb acceptance boundary.

The uncertainty associated with the luminosity determination is 3.9%, and the branching fraction uncertainty of the $J/\psi \rightarrow \mu^+\mu^-$ decay is 0.6%. The limited size of the simulated sample in each bin leads to an uncertainty between 0.3% and 5%, which is less than half of the data statistical uncertainty in each bin.

The detection efficiency is dependent on the polarisation of the J/ψ meson. Previous measurements by CDF [36] in $p\bar{p}$ collisions at 1.96 TeV, ALICE [28], CMS [29] and LHCb [30] in pp collisions at 7 TeV, showed that the prompt J/ψ polarisation in hadron collisions is small. The LHCb experiment studied J/ψ polarisation in the helicity frame [58] and measured the longitudinal polarisation parameter λ_θ [30] to be on average -0.145 ± 0.027 in the range $2 < p_T < 14$ GeV/ c and $2.0 < y < 4.5$. If the longitudinal polarisation is assumed to be -20% , the measured J/ψ cross-section would decrease by values between 0.7% and 6.2% depending on the J/ψ (p_T, y) bin, with an average value of 2.5%, which is smaller than the total systematic uncertainty. The efficiency changes in different p_T and y bins obtained under this assumption are discussed in the appendix. Therefore, since no polarisation measurement has yet been made for data collected at $\sqrt{s} = 13$ TeV, the polarisation is assumed to be zero, and no corresponding systematic uncertainty is quoted on the cross-section related to this effect.

There are sources of systematic uncertainties that are related to the t_z fit, that affect only J/ψ -from- b decays and are negligible for prompt J/ψ production. The modelling of the t_z resolution is studied by adding a third Gaussian to the nominal resolution model. The variation in F_b is found to be negligible. Background modelling is tested using the *sPlot* [59] method to extract the background t_z distribution and the relative variation in

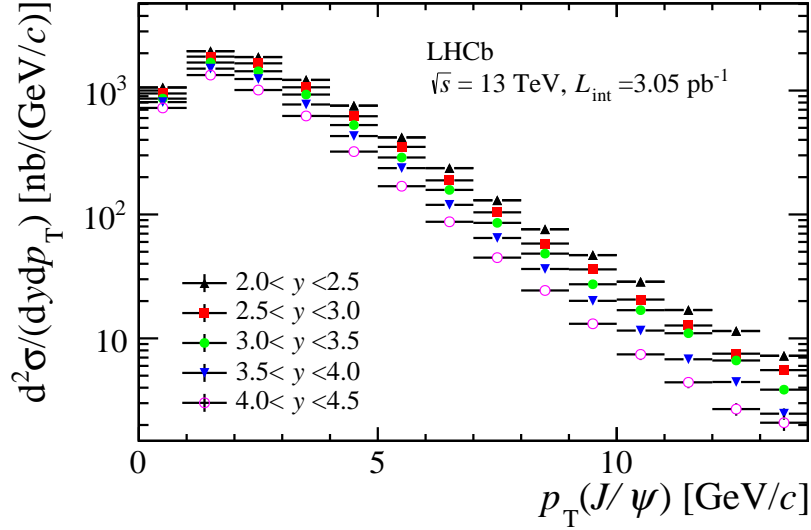


Figure 2: Double differential cross-section for prompt J/ψ mesons as a function of p_T in bins of y . Statistical and systematic uncertainties are added in quadrature.

F_b is taken as a systematic uncertainty. The impact of the choice of t_z parametrisation for the long tail component is studied using an exponential function with equal magnitude for positive and negative slopes and the relative difference of F_b is taken as a systematic uncertainty. The total relative systematic uncertainty on the J/ψ -from- b cross-section related to the t_z fit is 0.1%.

6 Results

The measured double differential cross-sections for prompt J/ψ and J/ψ -from- b mesons, assuming no polarisation, are shown in Figs. 2 and 3, and given in Tables 2 and 3. The cross-sections for prompt J/ψ and J/ψ -from- b mesons in the acceptance $p_T < 14$ GeV/ c and $2.0 < y < 4.5$, integrated over all (p_T, y) bins, are:

$$\begin{aligned} \sigma(\text{prompt } J/\psi, p_T < 14 \text{ GeV}/c, 2.0 < y < 4.5) &= 15.30 \pm 0.03 \pm 0.86 \mu\text{b}, \\ \sigma(J/\psi\text{-from-}b, p_T < 14 \text{ GeV}/c, 2.0 < y < 4.5) &= 2.34 \pm 0.01 \pm 0.13 \mu\text{b}, \end{aligned}$$

where the first uncertainties are statistical and the second systematic.

6.1 Fraction of J/ψ -from- b mesons

The fractions of J/ψ -from- b mesons in different kinematic bins are given in Fig. 4 and Table 6. The fraction increases as a function of p_T , and tends to decrease with increasing rapidity. These trends are consistent with the measurements at $\sqrt{s} = 7$ TeV and $\sqrt{s} =$

Table 2: Double differential production cross-section in nb/(GeV/c) for prompt J/ψ mesons in bins of (p_T, y) . The first uncertainties are statistical, the second are the correlated systematic uncertainties shared between bins and the last are the uncorrelated systematic uncertainties.

p_T [GeV/c]	$2.0 < y < 2.5$	$2.5 < y < 3.0$	$3.0 < y < 3.5$
0–1	1059 ± 16 ± 46 ± 32	947 ± 9 ± 38 ± 8	861 ± 8 ± 39 ± 5
1–2	2079 ± 22 ± 89 ± 17	1878 ± 12 ± 75 ± 11	1683 ± 10 ± 77 ± 6
2–3	1863 ± 18 ± 78 ± 17	1659 ± 11 ± 66 ± 13	1431 ± 9 ± 63 ± 5
3–4	1218 ± 13 ± 51 ± 14	1062 ± 7 ± 43 ± 6	928 ± 6 ± 39 ± 3
4–5	755 ± 9 ± 31 ± 9	620 ± 5 ± 25 ± 4	527 ± 4 ± 22 ± 2
5–6	419 ± 6 ± 17 ± 5	351 ± 3 ± 14 ± 2	288 ± 3 ± 12 ± 1
6–7	236.7 ± 3.7 ± 9.6 ± 7.4	188.4 ± 2.2 ± 7.5 ± 1.3	157.8 ± 1.9 ± 6.4 ± 0.9
7–8	130.2 ± 2.5 ± 5.3 ± 3.8	104.0 ± 1.6 ± 4.2 ± 0.8	85.6 ± 1.4 ± 3.4 ± 0.6
8–9	76.0 ± 1.8 ± 3.1 ± 1.4	58.2 ± 1.2 ± 2.3 ± 0.6	48.3 ± 1.0 ± 1.9 ± 0.4
9–10	47.0 ± 1.3 ± 1.9 ± 1.1	36.0 ± 0.9 ± 1.4 ± 0.4	27.3 ± 0.7 ± 1.1 ± 0.3
10–11	28.7 ± 1.0 ± 1.1 ± 0.6	20.6 ± 0.7 ± 0.8 ± 0.4	16.9 ± 0.6 ± 0.7 ± 0.2
11–12	16.9 ± 0.8 ± 0.7 ± 0.5	12.7 ± 0.5 ± 0.5 ± 0.2	11.0 ± 0.5 ± 0.4 ± 0.2
12–13	11.5 ± 0.6 ± 0.5 ± 0.4	7.5 ± 0.4 ± 0.3 ± 0.2	6.6 ± 0.4 ± 0.3 ± 0.1
13–14	7.2 ± 0.5 ± 0.3 ± 0.3	5.5 ± 0.3 ± 0.2 ± 0.1	3.9 ± 0.3 ± 0.2 ± 0.1
	$3.5 < y < 4.0$	$4.0 < y < 4.5$	
0–1	807 ± 7 ± 45 ± 5	724 ± 8 ± 48 ± 9	
1–2	1503 ± 9 ± 87 ± 6	1333 ± 11 ± 95 ± 17	
2–3	1239 ± 8 ± 69 ± 5	1010 ± 10 ± 73 ± 14	
3–4	772 ± 6 ± 40 ± 3	624 ± 8 ± 42 ± 11	
4–5	429 ± 4 ± 20 ± 2	322 ± 5 ± 19 ± 7	
5–6	237 ± 3 ± 11 ± 1	169 ± 3 ± 9 ± 3	
6–7	119.6 ± 1.7 ± 5.2 ± 0.8	87.3 ± 2.1 ± 4.5 ± 1.0	
7–8	64.6 ± 1.2 ± 2.8 ± 0.5	44.8 ± 1.4 ± 2.2 ± 1.3	
8–9	36.3 ± 0.9 ± 1.5 ± 0.3	24.4 ± 1.0 ± 1.2 ± 1.0	
9–10	20.1 ± 0.7 ± 0.8 ± 0.2	13.1 ± 0.7 ± 0.6 ± 0.4	
10–11	11.6 ± 0.5 ± 0.5 ± 0.2	7.4 ± 0.5 ± 0.3 ± 0.4	
11–12	6.8 ± 0.4 ± 0.3 ± 0.1	4.4 ± 0.4 ± 0.2 ± 0.2	
12–13	4.4 ± 0.3 ± 0.2 ± 0.1	2.7 ± 0.2 ± 0.1 ± 0.1	
13–14	2.5 ± 0.2 ± 0.1 ± 0.1	2.1 ± 0.2 ± 0.1 ± 0.1	

Table 3: Double differential production cross-section in nb/(GeV/c) for J/ψ -from- b mesons in bins of (p_T, y) . The first uncertainties are statistical, the second are the correlated systematic uncertainties shared between bins and the last are the uncorrelated systematic uncertainties.

p_T [GeV/c]	$2.0 < y < 2.5$	$2.5 < y < 3.0$	$3.0 < y < 3.5$
0–1	$113.2 \pm 5.4 \pm 6.7 \pm 3.7$	$102.3 \pm 2.9 \pm 5.3 \pm 1.1$	$92.7 \pm 2.6 \pm 5.0 \pm 0.8$
1–2	$276.3 \pm 6.9 \pm 15.5 \pm 3.4$	$243.6 \pm 3.9 \pm 12.4 \pm 2.0$	$209.3 \pm 3.3 \pm 11.4 \pm 1.3$
2–3	$300.6 \pm 6.4 \pm 16.2 \pm 4.1$	$249.4 \pm 3.6 \pm 12.6 \pm 2.5$	$204.5 \pm 3.0 \pm 10.9 \pm 1.3$
3–4	$238.6 \pm 5.3 \pm 12.6 \pm 4.0$	$186.8 \pm 2.9 \pm 9.4 \pm 1.7$	$152.4 \pm 2.4 \pm 7.8 \pm 1.1$
4–5	$159.9 \pm 3.8 \pm 8.3 \pm 2.9$	$126.3 \pm 2.1 \pm 6.3 \pm 1.3$	$97.2 \pm 1.7 \pm 4.9 \pm 0.8$
5–6	$103.3 \pm 2.8 \pm 5.3 \pm 1.9$	$78.5 \pm 1.5 \pm 3.9 \pm 0.9$	$59.2 \pm 1.3 \pm 3.0 \pm 0.6$
6–7	$67.9 \pm 2.0 \pm 3.4 \pm 2.4$	$52.1 \pm 1.2 \pm 2.6 \pm 0.7$	$38.0 \pm 1.0 \pm 1.9 \pm 0.4$
7–8	$42.9 \pm 1.5 \pm 2.2 \pm 1.5$	$31.2 \pm 0.9 \pm 1.6 \pm 0.5$	$24.3 \pm 0.8 \pm 1.2 \pm 0.3$
8–9	$25.3 \pm 1.1 \pm 1.3 \pm 0.7$	$21.9 \pm 0.7 \pm 1.1 \pm 0.4$	$15.2 \pm 0.6 \pm 0.8 \pm 0.3$
9–10	$18.9 \pm 0.9 \pm 0.9 \pm 0.7$	$12.8 \pm 0.5 \pm 0.6 \pm 0.3$	$10.3 \pm 0.5 \pm 0.5 \pm 0.2$
10–11	$14.2 \pm 0.8 \pm 0.7 \pm 0.5$	$9.1 \pm 0.5 \pm 0.5 \pm 0.2$	$6.7 \pm 0.4 \pm 0.3 \pm 0.2$
11–12	$9.0 \pm 0.6 \pm 0.4 \pm 0.4$	$6.8 \pm 0.4 \pm 0.3 \pm 0.2$	$4.3 \pm 0.3 \pm 0.2 \pm 0.1$
12–13	$6.5 \pm 0.5 \pm 0.3 \pm 0.3$	$4.5 \pm 0.3 \pm 0.2 \pm 0.2$	$3.3 \pm 0.3 \pm 0.2 \pm 0.1$
13–14	$4.9 \pm 0.4 \pm 0.2 \pm 0.3$	$3.6 \pm 0.3 \pm 0.2 \pm 0.1$	$2.4 \pm 0.2 \pm 0.1 \pm 0.1$
	$3.5 - 4.0$	$4.0 - 4.5$	
0–1	$83.4 \pm 2.7 \pm 5.3 \pm 0.8$	$64.9 \pm 3.8 \pm 4.7 \pm 1.1$	
1–2	$174.0 \pm 3.3 \pm 11.3 \pm 1.2$	$129.5 \pm 4.3 \pm 10.0 \pm 2.0$	
2–3	$168.5 \pm 2.9 \pm 10.6 \pm 1.3$	$121.2 \pm 3.7 \pm 9.4 \pm 2.1$	
3–4	$117.0 \pm 2.2 \pm 6.9 \pm 1.0$	$84.7 \pm 2.9 \pm 6.2 \pm 1.8$	
4–5	$76.7 \pm 1.6 \pm 4.3 \pm 0.7$	$50.5 \pm 2.0 \pm 3.3 \pm 1.3$	
5–6	$44.2 \pm 1.2 \pm 2.4 \pm 0.5$	$27.9 \pm 1.3 \pm 1.7 \pm 0.7$	
6–7	$26.7 \pm 0.9 \pm 1.4 \pm 0.4$	$17.2 \pm 1.0 \pm 1.0 \pm 0.4$	
7–8	$17.4 \pm 0.7 \pm 0.9 \pm 0.3$	$10.2 \pm 0.7 \pm 0.6 \pm 0.4$	
8–9	$9.2 \pm 0.5 \pm 0.5 \pm 0.2$	$6.1 \pm 0.5 \pm 0.3 \pm 0.3$	
9–10	$7.8 \pm 0.4 \pm 0.4 \pm 0.2$	$4.2 \pm 0.4 \pm 0.2 \pm 0.2$	
10–11	$4.7 \pm 0.3 \pm 0.2 \pm 0.1$	$3.1 \pm 0.3 \pm 0.2 \pm 0.2$	
11–12	$2.7 \pm 0.3 \pm 0.1 \pm 0.1$	$2.5 \pm 0.3 \pm 0.1 \pm 0.1$	
12–13	$1.8 \pm 0.2 \pm 0.1 \pm 0.1$	$0.9 \pm 0.2 \pm 0.1 \pm 0.1$	
13–14	$1.5 \pm 0.2 \pm 0.1 \pm 0.1$	$0.6 \pm 0.1 \pm 0.0 \pm 0.1$	

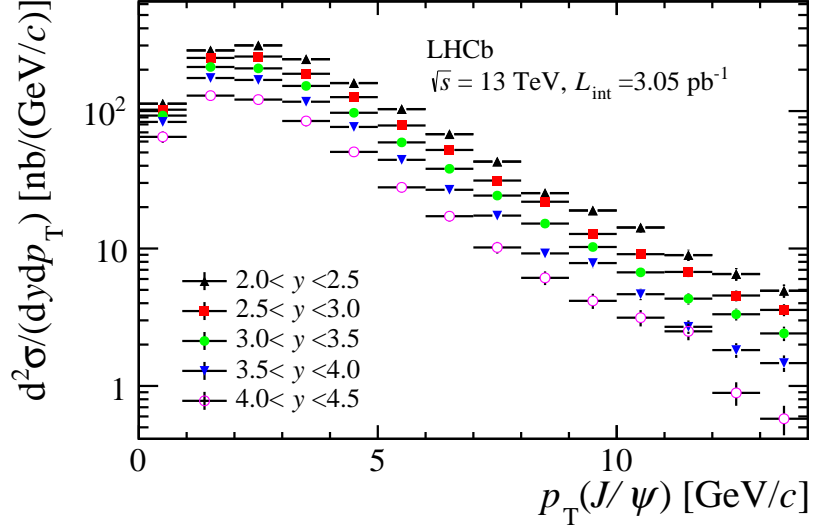


Figure 3: Double differential cross-section for J/ψ -from- b mesons as a function of p_T in bins of y . Statistical and systematic uncertainties are added in quadrature.

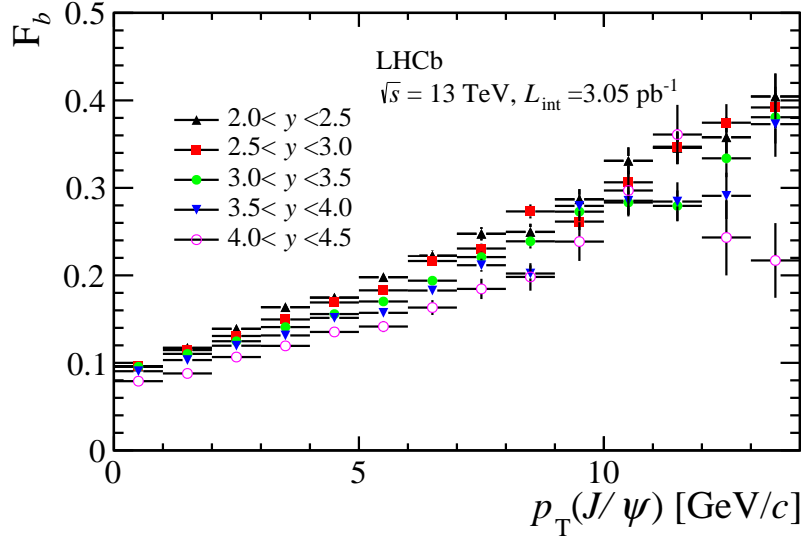


Figure 4: Fractions of J/ψ -from- b mesons in bins of J/ψ p_T and y . Statistical and systematic uncertainties are added in quadrature.

8 TeV [13,18]. A measurement of the non-prompt J/ψ production fraction at $\sqrt{s} = 13$ TeV has also been performed by the ATLAS collaboration [60].

6.2 Extrapolation to the total $b\bar{b}$ cross-section

The total $b\bar{b}$ production cross-section is calculated using:

$$\sigma(pp \rightarrow b\bar{b}X) = \alpha_{4\pi} \frac{\sigma(J/\psi\text{-from-}b, p_T < 14 \text{ GeV}/c, 2.0 < y < 4.5)}{2\mathcal{B}(b \rightarrow J/\psi X)}, \quad (3)$$

where $\alpha_{4\pi}$ is the extrapolation factor to the full kinematic region and $\mathcal{B}(b \rightarrow J/\psi X) = 1.16 \pm 0.10\%$ [43] is the inclusive $b \rightarrow J/\psi X$ branching fraction. Using the LHCb tuning of PYTHIA 6 [46], $\alpha_{4\pi}$ is found to be 5.2. The extrapolation predictions given by PYTHIA 8 and FONLL [27] are $\alpha_{4\pi} = 5.1$ and $\alpha_{4\pi} = 5.0$ respectively at $\sqrt{s} = 13$ TeV. Their predictions at $\sqrt{s} = 7$ TeV are compatible with the estimate using LHC J/ψ cross-section measurements in different rapidity ranges [17, 30]. Using the extrapolation factor from PYTHIA 6, the total $b\bar{b}$ production cross-section is found to be $\sigma(pp \rightarrow b\bar{b}X) = 515 \pm 2 \pm 53 \mu\text{b}$, where the first uncertainty is statistical and the second systematic. No uncertainty on $\alpha_{4\pi}$ is included in this estimate.

6.3 Comparison with lower energy results

The J/ψ cross-sections measured at $\sqrt{s} = 13$ TeV are compared to previous LHCb measurements [12, 18, 30]. In all previous LHCb measurements of the J/ψ production cross-section, the branching fraction from Ref. [61], $\mathcal{B}(J/\psi \rightarrow \mu^+\mu^-) = (5.94 \pm 0.06)\%$, was used. When the measurements at 13 TeV are compared with those at lower energy, the previous results are updated with the improved branching fraction value, $\mathcal{B}(J/\psi \rightarrow \mu^+\mu^-) = (5.961 \pm 0.033)\%$ [43]. The corresponding systematic uncertainty is totally correlated among the measurements. The differential cross-section as a function of p_T integrated over y is shown in Fig. 5, including all uncertainties, compared to measurements with pp collisions at $\sqrt{s} = 8$ TeV, for prompt J/ψ and J/ψ -from- b mesons. In Fig. 6, the differential cross-section as a function of y integrated over p_T is shown, compared to measurements with pp collisions at $\sqrt{s} = 8$ TeV. Tables 7 and 8 show the differential cross-sections integrated over y and p_T for prompt J/ψ and J/ψ -from- b mesons.

In Fig. 7, the ratios $R_{13/8}$ of the double differential cross-sections in pp collisions at $\sqrt{s} = 13$ TeV and at $\sqrt{s} = 8$ TeV are given for prompt J/ψ and J/ψ -from- b mesons, taking into account the correlations of various systematic uncertainties. The ratios of the cross-sections in bins of y integrated over p_T are shown in Fig. 8, while those in bins of p_T integrated over y are in Fig. 9. The cross-section ratios are summarised in Table 9 and 10 for prompt J/ψ and J/ψ -from- b respectively.

In the cross-section ratios, many of the systematic uncertainties cancel because of correlations between the two measurements. The uncertainty of the luminosity determination, which is the dominating systematic uncertainty, is determined to be 50% correlated [54], yielding a total uncertainty in the ratio of 4.6%. The uncertainties due to the signal mass shape, vertex fit quality requirement, radiative tail, muon identification, tracking efficiency, $J/\psi \rightarrow \mu^+\mu^-$ branching fraction and trigger are also totally or partially correlated. The remaining systematic uncertainties of the cross-section ratio are summarised in Table 4.

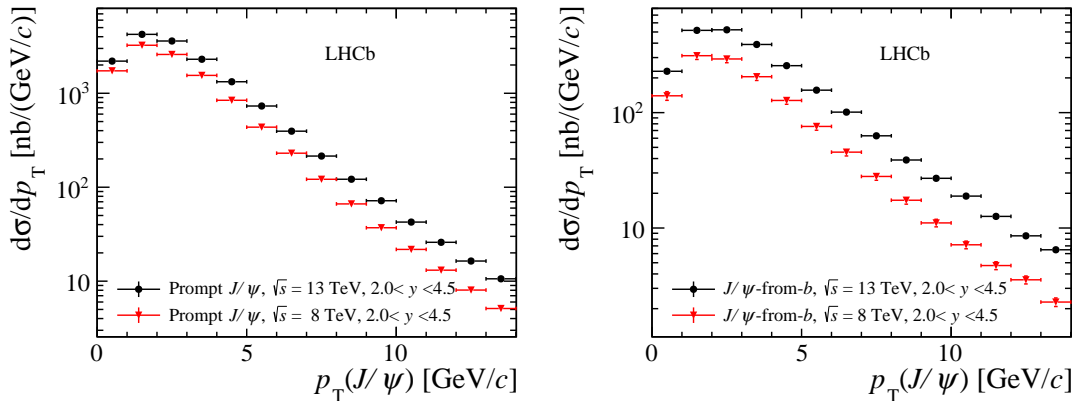


Figure 5: Differential cross-sections as a function of p_T integrated over y for (left) prompt J/ψ and (right) J/ψ -from- b mesons.

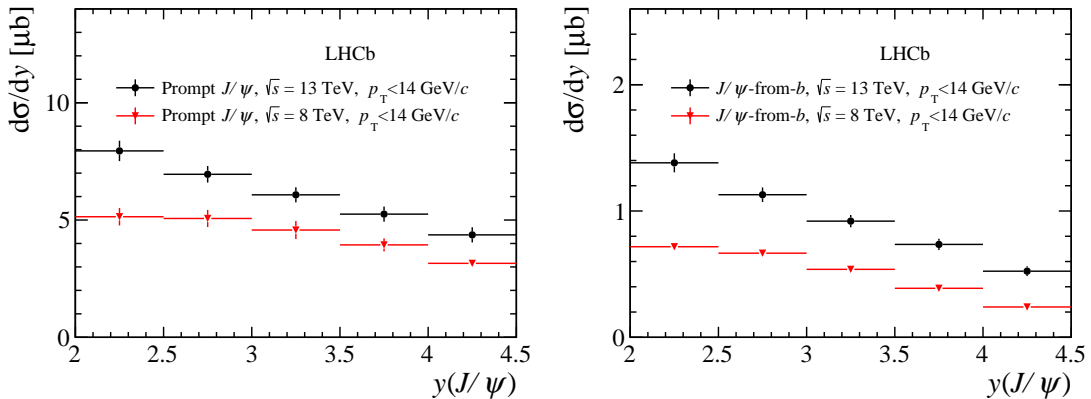


Figure 6: Differential cross-sections as a function of y integrated over p_T for (left) prompt J/ψ and (right) J/ψ -from- b mesons.

In Fig. 10 the total cross-section in the fiducial region $p_T < 14$ GeV/ c and $2.0 < y < 4.5$, as a function of pp centre-of-mass energy, is shown for prompt J/ψ and J/ψ -from- b mesons. The larger cross-section for J/ψ meson production at $\sqrt{s} = 13$ TeV compared to $\sqrt{s} = 8$ TeV is mostly due to the increased pp collision energy, but is also partly due to the increased boost of the produced b -hadron into the fiducial region. In Table 5, the cross-sections of prompt J/ψ and J/ψ -from- b mesons integrated over the kinematic range $2.0 < y < 4.5$, $p_T < 14$ GeV/ c ($p_T < 12$ GeV/ c for the analysis in pp at $\sqrt{s} = 2.76$ TeV) are given for pp collisions in different centre-of-mass energies. The cross-section values for pp collisions at $\sqrt{s} = 2.76$ TeV, $\sqrt{s} = 7$ TeV and $\sqrt{s} = 8$ TeV are taken from Refs. [12, 30] and [18]. The uncertainties are split into parts that are correlated and uncorrelated between the measurements at different pp centre-of-mass energies.

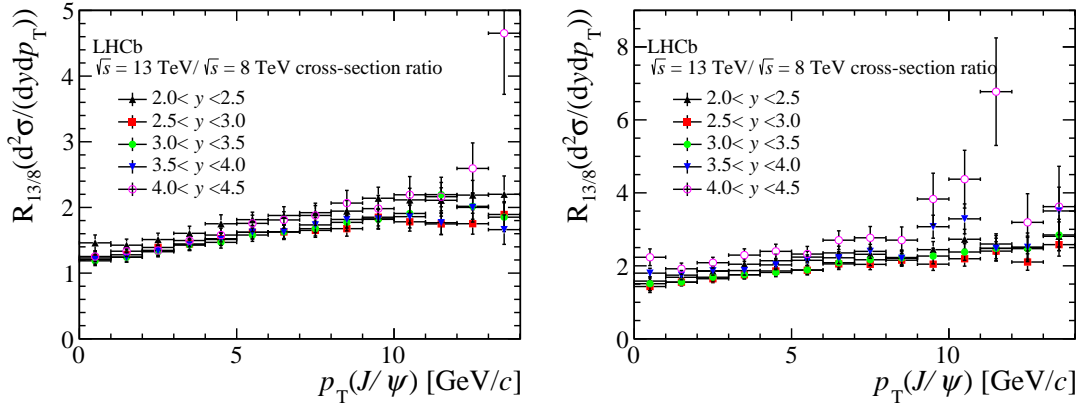


Figure 7: Ratios of differential cross-sections between measurements at $\sqrt{s} = 13$ TeV and $\sqrt{s} = 8$ TeV as a function of p_T in bins of y for (left) prompt J/ψ mesons and (right) J/ψ -from- b mesons.

6.4 Comparison with theoretical models

The measured J/ψ cross-sections are compared to the calculations of NRQCD and FONLL for prompt J/ψ and for J/ψ -from- b . Figure 11 (left) shows the comparison between the NRQCD calculation [63] and the measured prompt J/ψ cross-section as a function of transverse momentum, integrated over y in the range $2.0 < y < 4.5$. In the NRQCD

Table 4: Relative systematic uncertainty (in %) on the ratio of the cross-section in pp collisions at $\sqrt{s} = 13$ TeV relative to that at $\sqrt{s} = 8$ TeV. The systematic uncertainty from t_z fits only affects J/ψ -from- b .

Source	Systematic uncertainty (%)
Luminosity	4.6
Trigger	1.5
Muon ID	2.2
Tracking	1.0
Signal mass shape	2.0
p_T , y spectrum, simulation statistics (t_z fits)	1.0 – 8.0

Table 5: Production cross-sections of prompt J/ψ and J/ψ -from- b mesons, integrated over the LHCb fiducial region, in pp collisions at various centre-of-mass energies [12, 18, 30]. The first uncertainty is the uncorrelated component, and the second the correlated one.

σ_{tot} (μb)	$\sqrt{s} = 2.76$ TeV	$\sqrt{s} = 7$ TeV	$\sqrt{s} = 8$ TeV	$\sqrt{s} = 13$ TeV
Prompt J/ψ	$5.2 \pm 0.3 \pm 0.3$	$9.4 \pm 0.5^{+0.7}_{-1.0}$	$10.9 \pm 0.5 \pm 0.6$	$15.3 \pm 0.6 \pm 0.6$
J/ψ -from- b	$0.39 \pm 0.04 \pm 0.04$	$1.07 \pm 0.05 \pm 0.06$	$1.27 \pm 0.06 \pm 0.09$	$2.34 \pm 0.09 \pm 0.09$

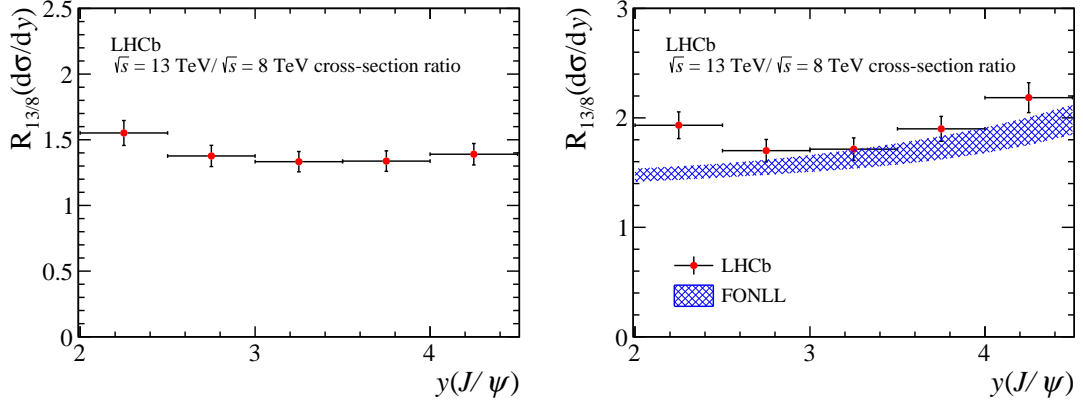


Figure 8: Ratios of differential cross-sections between measurements at $\sqrt{s} = 13$ TeV and $\sqrt{s} = 8$ TeV as a function of y integrated over p_T for (left) prompt J/ψ and (right) J/ψ -from- b mesons. The FONLL calculation [62] is compared to the measured J/ψ -from- b production ratio.

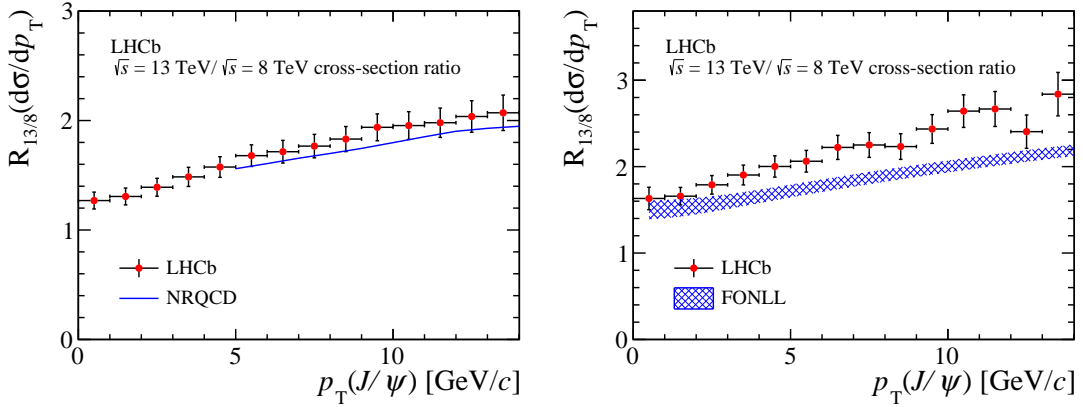


Figure 9: Ratios of differential cross-sections between measurements at $\sqrt{s} = 13$ TeV and $\sqrt{s} = 8$ TeV as a function of p_T integrated over y for (left) prompt J/ψ mesons and (right) J/ψ -from- b mesons. Calculations of NRQCD [63] and FONLL [62] are compared to prompt J/ψ mesons and J/ψ -from- b mesons, respectively.

calculation, only uncertainties associated with LDME are considered since these are the dominating uncertainties for the absolute production cross-section prediction. The FONLL calculation [27] is compared to the measurements of the J/ψ -from- b cross-section as a function of transverse momentum integrated over y in the range $2.0 < y < 4.5$ in Fig. 11 (right). The FONLL calculation includes the uncertainties due to the b -quark mass and the renormalisation and factorisation scales for the prediction of the absolute production cross-section. Good agreement is found between the measurements and the theoretical calculations.

Fig. 8 (right) shows the ratio of the cross-sections as a function of y integrated over p_T

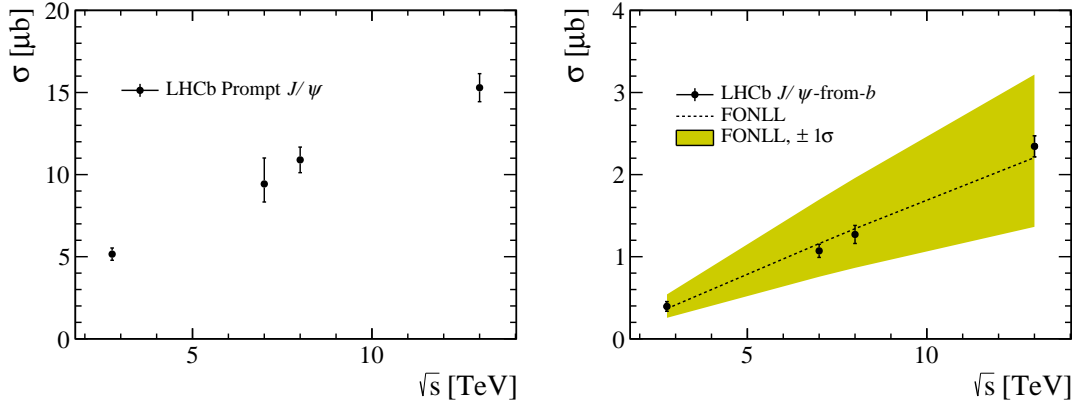


Figure 10: The J/ψ production cross-section for (left) prompt J/ψ and (right) J/ψ -from- b mesons as a function of pp collision energy in the LHCb fiducial region compared to the FONLL calculation [27]. In general, the correlated and uncorrelated systematic uncertainties among different measurements are of comparable magnitude.

in the range $p_T < 14 \text{ GeV}/c$ is compared with the FONLL calculation based on Ref. [62] for J/ψ -from- b . The ratio of the cross-sections as a function of p_T integrated over y in the range $2.0 < y < 4.5$ is compared with the NRQCD calculation [63] for prompt J/ψ mesons, and with predictions by FONLL based on Ref. [62] for J/ψ -from- b , shown in Fig. 9. The uncertainty of the NRQCD prediction, considering only that from LDME, almost cancels in the cross-section ratio between the 13 TeV and 8 TeV measurements, so no uncertainty is given for the calculations in Fig. 9 (left). Besides those due to the b -quark mass and the scales, the FONLL calculation for the cross-section ratio also takes into account the gluon PDF uncertainty. The NRQCD prediction agrees reasonably well with the experimental data for the prompt J/ψ production cross-section ratio, while the FONLL prediction is below the J/ψ -from- b meson measurements.

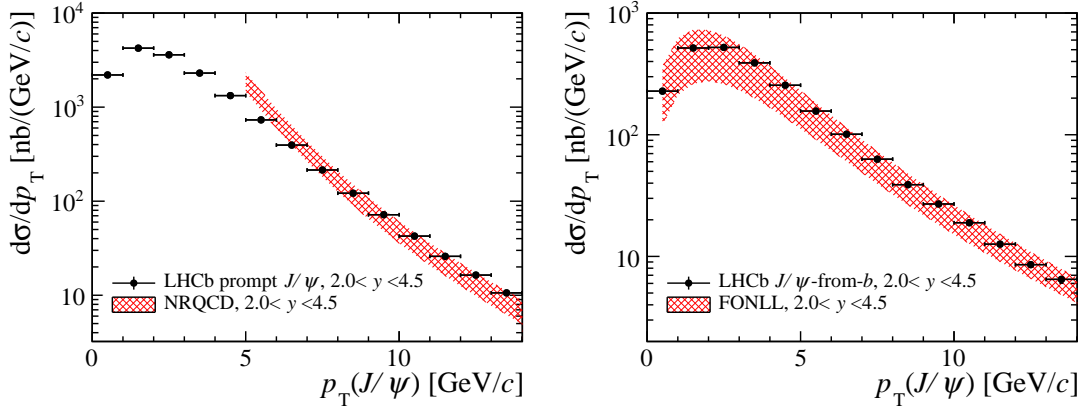


Figure 11: Differential cross-sections as a function of p_T integrated over y in the range $2.0 < y < 4.5$, (left) compared with the NRQCD calculation [63] for prompt J/ψ and (right) compared with the FONLL calculation [27] for J/ψ -from- b mesons.

Table 6: The fraction of J/ψ -from- b mesons (in %) in bins of the J/ψ transverse momentum and rapidity. The uncertainties are statistical only. The systematic uncertainties are negligible.

p_T [GeV/c]	$2.0 < y < 2.5$	$2.5 < y < 3.0$	$3.0 < y < 3.5$	$3.5 < y < 4.0$	$4.0 < y < 4.5$
0 – 1	9.6 ± 0.4	9.6 ± 0.3	9.6 ± 0.3	9.0 ± 0.3	7.9 ± 0.5
1 – 2	11.7 ± 0.3	11.5 ± 0.2	11.0 ± 0.2	10.3 ± 0.2	8.8 ± 0.3
2 – 3	13.9 ± 0.3	13.1 ± 0.2	12.5 ± 0.2	12.0 ± 0.2	10.7 ± 0.3
3 – 4	16.4 ± 0.3	15.0 ± 0.2	14.1 ± 0.2	13.1 ± 0.2	11.9 ± 0.4
4 – 5	17.5 ± 0.4	16.9 ± 0.3	15.6 ± 0.3	15.1 ± 0.3	13.5 ± 0.5
5 – 6	19.8 ± 0.5	18.3 ± 0.3	17.0 ± 0.3	15.7 ± 0.4	14.2 ± 0.6
6 – 7	22.2 ± 0.6	21.6 ± 0.5	19.4 ± 0.5	18.3 ± 0.5	16.3 ± 0.9
7 – 8	24.8 ± 0.8	23.1 ± 0.6	22.1 ± 0.6	21.2 ± 0.7	18.5 ± 1.2
8 – 9	25.0 ± 0.9	27.3 ± 0.8	23.9 ± 0.8	20.2 ± 0.9	19.8 ± 1.6
9 – 10	28.7 ± 1.2	26.1 ± 1.0	27.3 ± 1.1	27.9 ± 1.3	23.9 ± 2.2
10 – 11	33.1 ± 1.5	30.6 ± 1.3	28.3 ± 1.4	28.5 ± 1.8	29.7 ± 2.8
11 – 12	34.6 ± 1.9	34.7 ± 1.6	27.9 ± 1.8	28.4 ± 2.2	36.1 ± 3.4
12 – 13	35.8 ± 2.3	37.4 ± 2.1	33.4 ± 2.2	29.1 ± 2.6	24.3 ± 4.3
13 – 14	40.4 ± 2.6	39.2 ± 2.4	38.1 ± 3.0	37.3 ± 3.7	21.7 ± 4.3

Table 7: Differential cross-sections $d\sigma/dp_T$ (in nb/(GeV/c)) for prompt J/ψ and J/ψ -from- b mesons, integrated over y . The first uncertainties are statistical and the second (third) are uncorrelated (correlated) systematic uncertainties amongst bins.

p_T [GeV/c]	Prompt J/ψ	J/ψ -from- b
0–1	$2198 \pm 11 \pm 17 \pm 127$	$228.3 \pm 4.1 \pm 1.8 \pm 13.1$
1–2	$4237 \pm 15 \pm 13 \pm 245$	$516.4 \pm 5.1 \pm 1.7 \pm 29.5$
2–3	$3600 \pm 12 \pm 13 \pm 202$	$522.1 \pm 4.6 \pm 2.0 \pm 29.1$
3–4	$2301 \pm 9 \pm 99 \pm 125$	$389.7 \pm 3.7 \pm 1.7 \pm 21.0$
4–5	$1326 \pm 6 \pm 96 \pm 69$	$255.2 \pm 2.7 \pm 1.3 \pm 13.4$
5–6	$731.8 \pm 4.0 \pm 3.1 \pm 37.9$	$156.6 \pm 1.9 \pm 0.7 \pm 8.1$
6–7	$394.9 \pm 2.7 \pm 3.8 \pm 20.3$	$101.0 \pm 1.4 \pm 1.1 \pm 5.2$
7–8	$214.6 \pm 1.9 \pm 2.1 \pm 10.9$	$63.0 \pm 1.1 \pm 0.7 \pm 3.2$
8–9	$121.6 \pm 1.4 \pm 0.9 \pm 6.2$	$38.9 \pm 0.8 \pm 0.3 \pm 2.0$
9–10	$71.8 \pm 1.0 \pm 0.7 \pm 3.6$	$27.0 \pm 0.7 \pm 0.3 \pm 1.4$
10–11	$42.6 \pm 0.8 \pm 0.4 \pm 2.2$	$18.9 \pm 0.6 \pm 0.2 \pm 1.0$
11–12	$25.9 \pm 0.6 \pm 0.3 \pm 1.3$	$12.6 \pm 0.4 \pm 0.1 \pm 0.6$
12–13	$16.4 \pm 0.5 \pm 0.2 \pm 0.8$	$8.6 \pm 0.3 \pm 0.1 \pm 0.4$
13–14	$10.6 \pm 0.4 \pm 0.2 \pm 0.5$	$6.5 \pm 0.3 \pm 0.1 \pm 0.3$

Table 8: Differential cross-sections $d\sigma/dy$ (in μb) for prompt J/ψ and J/ψ -from- b mesons, integrated over p_T . The first uncertainties are statistical and the second (third) are the uncorrelated (correlated) systematic uncertainties.

y	Prompt J/ψ	J/ψ -from- b
2.0 – 2.5	$7.947 \pm 0.036 \pm 0.044 \pm 0.430$	$1.381 \pm 0.013 \pm 0.006 \pm 0.073$
2.5 – 3.0	$6.949 \pm 0.020 \pm 0.020 \pm 0.351$	$1.128 \pm 0.007 \pm 0.003 \pm 0.056$
3.0 – 3.5	$6.074 \pm 0.017 \pm 0.010 \pm 0.320$	$0.919 \pm 0.006 \pm 0.001 \pm 0.048$
3.5 – 4.0	$5.251 \pm 0.016 \pm 0.009 \pm 0.322$	$0.735 \pm 0.006 \pm 0.001 \pm 0.044$
4.0 – 4.5	$4.367 \pm 0.019 \pm 0.027 \pm 0.321$	$0.523 \pm 0.007 \pm 0.003 \pm 0.037$

Table 9: The ratio of cross-sections between measurements at 13 TeV and 8 TeV in different bins of p_T and y for prompt J/ψ mesons. The systematic errors are negligible.

p_T [GeV/c]	$2.0 < y < 2.5$	$2.5 < y < 3.0$	$3.0 < y < 3.5$	$3.5 < y < 4.0$	$4.0 < y < 4.5$	$2.0 < y < 4.5$
0 – 1	1.46 ± 0.12	1.23 ± 0.08	1.19 ± 0.07	1.21 ± 0.07	1.25 ± 0.08	1.27 ± 0.08
1 – 2	1.43 ± 0.09	1.28 ± 0.08	1.24 ± 0.07	1.24 ± 0.08	1.33 ± 0.08	1.31 ± 0.08
2 – 3	1.51 ± 0.10	1.39 ± 0.09	1.33 ± 0.08	1.34 ± 0.08	1.35 ± 0.08	1.39 ± 0.08
3 – 4	1.61 ± 0.11	1.44 ± 0.09	1.43 ± 0.08	1.43 ± 0.08	1.50 ± 0.09	1.49 ± 0.09
4 – 5	1.75 ± 0.14	1.52 ± 0.09	1.47 ± 0.09	1.51 ± 0.09	1.58 ± 0.10	1.58 ± 0.09
5 – 6	1.81 ± 0.11	1.62 ± 0.10	1.58 ± 0.10	1.62 ± 0.10	1.76 ± 0.12	1.68 ± 0.10
6 – 7	1.88 ± 0.13	1.63 ± 0.11	1.63 ± 0.10	1.63 ± 0.10	1.81 ± 0.13	1.72 ± 0.10
7 – 8	1.92 ± 0.14	1.65 ± 0.11	1.68 ± 0.11	1.73 ± 0.12	1.88 ± 0.15	1.77 ± 0.11
8 – 9	1.94 ± 0.16	1.68 ± 0.11	1.77 ± 0.13	1.82 ± 0.13	2.07 ± 0.19	1.83 ± 0.11
9 – 10	2.14 ± 0.17	1.85 ± 0.13	1.82 ± 0.15	1.83 ± 0.15	1.98 ± 0.20	1.94 ± 0.12
10 – 11	2.11 ± 0.18	1.78 ± 0.14	1.91 ± 0.15	1.86 ± 0.17	2.19 ± 0.28	1.95 ± 0.13
11 – 12	2.11 ± 0.19	1.75 ± 0.16	2.20 ± 0.18	1.77 ± 0.18	2.16 ± 0.30	1.98 ± 0.13
12 – 13	2.19 ± 0.22	1.75 ± 0.16	2.02 ± 0.20	2.00 ± 0.22	2.59 ± 0.39	2.04 ± 0.14
13 – 14	2.20 ± 0.28	1.89 ± 0.20	1.85 ± 0.22	1.66 ± 0.22	4.65 ± 0.93	2.07 ± 0.16
0 – 14	1.55 ± 0.09	1.38 ± 0.08	1.33 ± 0.08	1.34 ± 0.08	1.39 ± 0.08	—

Table 10: The ratio of cross-sections between measurements at 13 TeV and 8 TeV in different bins of p_T and y for J/ψ -from- b mesons. The systematic errors are negligible.

p_T [(GeV/c)]	$2.0 < y < 2.5$	$2.5 < y < 3.0$	$3.0 < y < 3.5$	$3.5 < y < 4.0$	$4.0 < y < 4.5$	$2.0 < y < 4.5$
0 – 1	1.58 ± 0.25	1.43 ± 0.16	1.51 ± 0.19	1.80 ± 0.13	2.23 ± 0.23	1.63 ± 0.13
1 – 2	1.69 ± 0.12	1.55 ± 0.10	1.55 ± 0.10	1.74 ± 0.13	1.92 ± 0.16	1.66 ± 0.10
2 – 3	1.85 ± 0.13	1.65 ± 0.11	1.69 ± 0.11	1.86 ± 0.12	2.08 ± 0.15	1.79 ± 0.11
3 – 4	2.04 ± 0.15	1.75 ± 0.11	1.76 ± 0.11	1.87 ± 0.12	2.29 ± 0.17	1.90 ± 0.11
4 – 5	2.14 ± 0.18	1.86 ± 0.12	1.82 ± 0.12	2.03 ± 0.13	2.40 ± 0.20	2.00 ± 0.12
5 – 6	2.24 ± 0.16	1.88 ± 0.13	1.89 ± 0.13	2.15 ± 0.15	2.32 ± 0.21	2.06 ± 0.13
6 – 7	2.35 ± 0.18	2.05 ± 0.15	2.08 ± 0.14	2.22 ± 0.16	2.70 ± 0.26	2.22 ± 0.14
7 – 8	2.32 ± 0.19	2.04 ± 0.15	2.17 ± 0.16	2.40 ± 0.19	2.77 ± 0.31	2.25 ± 0.14
8 – 9	2.23 ± 0.21	2.15 ± 0.17	2.22 ± 0.19	2.21 ± 0.20	2.70 ± 0.36	2.23 ± 0.15
9 – 10	2.44 ± 0.22	2.05 ± 0.17	2.27 ± 0.21	3.07 ± 0.32	3.83 ± 0.71	2.44 ± 0.17
10 – 11	2.73 ± 0.27	2.19 ± 0.20	2.38 ± 0.23	3.29 ± 0.41	4.37 ± 0.79	2.64 ± 0.19
11 – 12	2.60 ± 0.28	2.40 ± 0.26	2.48 ± 0.28	2.48 ± 0.35	6.77 ± 1.47	2.67 ± 0.20
12 – 13	2.51 ± 0.31	2.10 ± 0.23	2.47 ± 0.31	2.51 ± 0.39	3.19 ± 0.78	2.40 ± 0.19
13 – 14	2.81 ± 0.39	2.58 ± 0.32	2.85 ± 0.43	3.50 ± 0.65	3.62 ± 1.11	2.84 ± 0.25
0 – 14	1.93 ± 0.12	1.70 ± 0.10	1.71 ± 0.10	1.90 ± 0.11	2.18 ± 0.14	—

7 Conclusions

The differential J/ψ production cross-section in pp collisions at $\sqrt{s} = 13$ TeV is measured as a function of the J/ψ transverse momentum and rapidity in the range of $p_T < 14$ GeV and $2.0 < y < 4.5$. The analysis is based on a data sample corresponding to an integrated luminosity of $3.05 \pm 0.12 \text{ pb}^{-1}$, collected with the LHCb detector in July 2015. The production cross-sections of prompt J/ψ and J/ψ -from- b mesons are measured separately. The ratios of the J/ψ cross-sections in pp collisions at a centre-of-mass energy of 13 TeV relative to those at 8 TeV are also determined.

The p_T distribution of J/ψ mesons produced in $\sqrt{s} = 13$ TeV pp collisions is harder than at $\sqrt{s} = 8$ TeV. The measured prompt J/ψ meson production cross-section as a function of transverse momentum is in good agreement with theoretical calculations in the NRQCD framework. Theoretical predictions based on FONLL calculations describe well the measured cross-section for J/ψ -from- b mesons and its dependence on the centre-of-mass energy of pp collisions, though the prediction lies below the ratio between the cross-section measurements at $\sqrt{s} = 13$ TeV and $\sqrt{s} = 8$ TeV.

Acknowledgements

The authors would like to thank K.-T. Chao, H. Han and H.-S. Shao for providing the NRQCD calculations, and M. Cacciari, M. L. Mangano and P. Nason for the FONLL predictions that are compared with the measurements discussed in the paper. We express our gratitude to our colleagues in the CERN accelerator departments for the excellent performance of the LHC. We thank the technical and administrative staff at the LHCb institutes. We acknowledge support from CERN and from the national agencies: CAPES, CNPq, FAPERJ and FINEP (Brazil); NSFC (China); CNRS/IN2P3 (France); BMBF, DFG, HGF and MPG (Germany); INFN (Italy); FOM and NWO (The Netherlands); MNiSW and NCN (Poland); MEN/IFA (Romania); MinES and FANO (Russia); MinECo (Spain); SNSF and SER (Switzerland); NASU (Ukraine); STFC (United Kingdom); NSF (USA). The Tier1 computing centres are supported by IN2P3 (France), KIT and BMBF (Germany), INFN (Italy), NWO and SURF (The Netherlands), PIC (Spain), GridPP (United Kingdom). We are indebted to the communities behind the multiple open source software packages on which we depend. We are also thankful for the computing resources and the access to software R&D tools provided by Yandex LLC (Russia). Individual groups or members have received support from EPLANET, Marie Skłodowska-Curie Actions and ERC (European Union), Conseil général de Haute-Savoie, Labex ENIGMASS and OCEVU, Région Auvergne (France), RFBR (Russia), XuntaGal and GENCAT (Spain), Royal Society and Royal Commission for the Exhibition of 1851 (United Kingdom).

References

- [1] C. E. Carlson and R. Suaya, *Hadronic production of the ψ/J meson*, Phys. Rev. **D14** (1976) 3115.
- [2] A. Donnachie and P. V. Landshoff, *Production of lepton pairs, J/ψ and charm with hadron beams*, Nucl. Phys. **B112** (1976) 233.
- [3] S. D. Ellis, M. B. Einhorn, and C. Quigg, *Comment on hadronic production of psions*, Phys. Rev. Lett. **36** (1976) 1263.
- [4] H. Fritzsch, *Producing heavy quark flavors in hadronic collisions: A test of quantum chromodynamics*, Phys. Lett. **B67** (1977) 217.
- [5] M. Gluck, J. F. Owens, and E. Reya, *Gluon contribution to hadronic J/ψ production*, Phys. Rev. **D17** (1978) 2324.
- [6] C.-H. Chang, *Hadronic production of J/ψ associated with a gluon*, Nucl. Phys. **B172** (1980) 425.
- [7] R. Baier and R. Rückl, *Hadronic production of J/ψ and Υ : Transverse momentum distributions*, Phys. Lett. **B102** (1981) 364.
- [8] G. T. Bodwin, E. Braaten, and G. P. Lepage, *Rigorous QCD analysis of inclusive annihilation and production of heavy quarkonium*, Phys. Rev. **D51** (1995) 1125, [arXiv:hep-ph/9407339](#).
- [9] P. L. Cho and A. K. Leibovich, *Color-octet quarkonia production*, Phys. Rev. **D53** (1996) 150, [arXiv:hep-ph/9505329](#).
- [10] P. L. Cho and A. K. Leibovich, *Color-octet quarkonia production. II.*, Phys. Rev. **D53** (1996) 6203, [arXiv:hep-ph/9511315](#).
- [11] ALICE collaboration, B. Abelev *et al.*, *Inclusive J/ψ production in pp collisions at $\sqrt{s} = 2.76$ TeV*, Phys. Lett. **B718** (2012) 295, [arXiv:1203.3641](#).
- [12] LHCb collaboration, R. Aaij *et al.*, *Measurement of J/ψ production in pp collisions at $\sqrt{s} = 2.76$ TeV*, JHEP **02** (2013) 041, [arXiv:1212.1045](#).
- [13] LHCb collaboration, R. Aaij *et al.*, *Measurement of J/ψ production in pp collisions at $\sqrt{s} = 7$ TeV*, Eur. Phys. J. **C71** (2011) 1645, [arXiv:1103.0423](#).
- [14] CMS collaboration, V. Khachatryan *et al.*, *Prompt and non-prompt J/ψ production in pp collisions at $\sqrt{s} = 7$ TeV*, Eur. Phys. J. **C71** (2011) 1575, [arXiv:1011.4193](#).
- [15] ATLAS collaboration, G. Aad *et al.*, *Measurement of the differential cross-sections of inclusive, prompt and non-prompt J/ψ production in proton-proton collisions at $\sqrt{s} = 7$ TeV*, Nucl. Phys. **B850** (2011) 387, [arXiv:1104.3038](#).

- [16] ALICE collaboration, K. Aamodt *et al.*, *Rapidity and transverse momentum dependence of inclusive J/ψ production in pp collisions at $\sqrt{s} = 7$ TeV*, Phys. Lett. **B704** (2011) 442, arXiv:1105.0380.
- [17] CMS collaboration, S. Chatrchyan *et al.*, *J/ψ and $\psi(2S)$ production in pp collisions at $\sqrt{s} = 7$ TeV*, JHEP **02** (2012) 011, arXiv:1111.1557.
- [18] LHCb collaboration, R. Aaij *et al.*, *Production of J/ψ and Υ mesons in pp collisions at $\sqrt{s} = 8$ TeV*, JHEP **06** (2013) 064, arXiv:1304.6977.
- [19] J. M. Campbell, F. Maltoni, and F. Tramontano, *QCD corrections to J/ψ and Υ production at hadron colliders*, Phys. Rev. Lett. **98** (2007) 252002, arXiv:hep-ph/0703113.
- [20] J. P. Lansberg, *J/ψ production at $\sqrt{s}=1.96$ and 7 TeV: Color-Singlet Model, NNLO* and polarisation*, J. Phys. **G38** (2011) 124110, arXiv:1107.0292.
- [21] CDF collaboration, F. Abe *et al.*, *Inclusive J/ψ , $\psi(2S)$ and b quark production in $\bar{p}p$ collisions at $\sqrt{s} = 1.8$ TeV*, Phys. Rev. Lett. **69** (1992) 3704.
- [22] M. Cacciari, M. Greco, M. L. Mangano, and A. Petrelli, *Charmonium production at the Tevatron*, Phys. Lett. **B356** (1995) 553, arXiv:hep-ph/9505379.
- [23] E. Braaten and S. Fleming, *Color-octet fragmentation and the ψ' surplus at the Fermilab Tevatron*, Phys. Rev. Lett. **74** (1995) 3327, arXiv:hep-ph/9411365.
- [24] Y.-Q. Ma, K. Wang, and K.-T. Chao, *Complete next-to-leading order calculation of the J/ψ and ψ' production at hadron colliders*, Phys. Rev. **D84** (2011) 114001, arXiv:1012.1030.
- [25] B. Gong, X. Q. Li, and J.-X. Wang, *QCD corrections to J/ψ production via color-octet states at Tevatron and LHC*, Phys. Lett. **B673** (2009) 197, arXiv:0805.4751.
- [26] M. Butenschoen and B. A. Kniehl, *Reconciling J/ψ production at HERA, RHIC, Tevatron, and LHC with nonrelativistic QCD factorization at next-to-leading order*, Phys. Rev. Lett. **106** (2011) 022003, arXiv:1009.5662.
- [27] M. Cacciari, M. Greco, and P. Nason, *The p_T spectrum in heavy flavor hadroproduction*, JHEP **05** (1998) 007, arXiv:hep-ph/9803400.
- [28] ALICE collaboration, B. Abelev *et al.*, *J/ψ polarization in pp collisions at $\sqrt{s} = 7$ TeV*, Phys. Rev. Lett. **108** (2012) 082001, arXiv:1111.1630.
- [29] CMS collaboration, S. Chatrchyan *et al.*, *Measurement of the prompt J/ψ and $\psi(2S)$ polarizations in pp collisions at $\sqrt{s} = 7$ TeV*, Phys. Lett. **B727** (2013) 381, arXiv:1307.6070.

- [30] LHCb collaboration, R. Aaij *et al.*, *Measurement of J/ψ polarization in pp collisions at $\sqrt{s} = 7$ TeV*, Eur. Phys. J. **C73** (2013) 2631, [arXiv:1307.6379](#).
- [31] B. Gong and J.-X. Wang, *Next-to-leading-order QCD corrections to J/ψ polarization at Tevatron and Large-Hadron-Collider energies*, Phys. Rev. Lett. **100** (2008) 232001, [arXiv:0802.3727](#).
- [32] M. Beneke and I. Z. Rothstein, *ψ' polarization as a test of colour octet quarkonium production*, Phys. Lett. **B372** (1996) 157, [arXiv:hep-ph/9509375](#).
- [33] K.-T. Chao *et al.*, *J/ψ polarization at hadron colliders in nonrelativistic QCD*, Phys. Rev. Lett. **108** (2012) 242004, [arXiv:1201.2675](#).
- [34] B. Gong, L.-P. Wan, J.-X. Wang, and H.-F. Zhang, *Polarization for prompt J/ψ and $\psi(2S)$ production at the Tevatron and LHC*, Phys. Rev. Lett. **110** (2013) 042002, [arXiv:1205.6682](#).
- [35] M. Butenschoen and B. A. Kniehl, *J/ψ polarization at Tevatron and LHC: Nonrelativistic-QCD factorization at the crossroads*, Phys. Rev. Lett. **108** (2012) 172002, [arXiv:1201.1872](#).
- [36] CDF collaboration, A. Abulencia *et al.*, *Polarization of J/ψ and $\psi(2S)$ mesons produced in $p\bar{p}$ collisions at $\sqrt{s} = 1.96$ TeV*, Phys. Rev. Lett. **99** (2007) 132001, [arXiv:0704.0638](#).
- [37] D0 collaboration, V. M. Abazov *et al.*, *Measurement of the polarization of the $\Upsilon(1S)$ and $\Upsilon(2S)$ states in $p\bar{p}$ collisions at $\sqrt{s} = 1.96$ TeV*, Phys. Rev. Lett. **101** (2008) 182004, [arXiv:0804.2799](#).
- [38] CMS collaboration, S. Chatrchyan *et al.*, *Measurement of the $\Upsilon(1S)$, $\Upsilon(2S)$ and $\Upsilon(3S)$ polarizations in pp collisions at $\sqrt{s} = 7$ TeV*, Phys. Rev. Lett. **110** (2013) 081802, [arXiv:1209.2922](#).
- [39] LHCb collaboration, R. Aaij *et al.*, *Measurement of $\psi(2S)$ polarisation in pp collisions at $\sqrt{s} = 7$ TeV*, Eur. Phys. J. **C74** (2014) 2872, [arXiv:1403.1339](#).
- [40] LHCb collaboration, A. A. Alves Jr. *et al.*, *The LHCb detector at the LHC*, JINST **3** (2008) S08005.
- [41] LHCb collaboration, R. Aaij *et al.*, *LHCb detector performance*, Int. J. Mod. Phys. **A30** (2015) 1530022, [arXiv:1412.6352](#).
- [42] A. A. Alves Jr. *et al.*, *Performance of the LHCb muon system*, JINST **8** (2013) P02022, [arXiv:1211.1346](#).
- [43] Particle Data Group, K. A. Olive *et al.*, *Review of particle physics*, Chin. Phys. **C38** (2014) 090001.

- [44] G. Dujany and B. Storaci, *Real-time alignment and calibration of the LHCb Detector in Run II*, LHCb-PROC-2015-011.
- [45] R. Aaij *et al.*, *The LHCb trigger and its performance in 2011*, JINST **8** (2013) P04022, arXiv:1211.3055.
- [46] T. Sjöstrand, S. Mrenna, and P. Skands, *PYTHIA 6.4 physics and manual*, JHEP **05** (2006) 026, arXiv:hep-ph/0603175.
- [47] I. Belyaev *et al.*, *Handling of the generation of primary events in Gauss, the LHCb simulation framework*, J. Phys. Conf. Ser. **331** (2011) 032047.
- [48] D. J. Lange, *The EvtGen particle decay simulation package*, Nucl. Instrum. Meth. **A462** (2001) 152.
- [49] P. Golonka and Z. Was, *PHOTOS Monte Carlo: A precision tool for QED corrections in Z and W decays*, Eur. Phys. J. **C45** (2006) 97, arXiv:hep-ph/0506026.
- [50] M. Bargiotti and V. Vagnoni, *Heavy quarkonia sector in PYTHIA 6.324: Tuning, validation and perspectives at LHC(b)*, CERN-LHCb-2007-042.
- [51] Geant4 collaboration, J. Allison *et al.*, *Geant4 developments and applications*, IEEE Trans. Nucl. Sci. **53** (2006) 270; Geant4 collaboration, S. Agostinelli *et al.*, *Geant4: A simulation toolkit*, Nucl. Instrum. Meth. **A506** (2003) 250.
- [52] M. Clemencic *et al.*, *The LHCb simulation application, Gauss: Design, evolution and experience*, J. Phys. Conf. Ser. **331** (2011) 032023.
- [53] C. Barschel, *Precision luminosity measurement at LHCb with beam-gas imaging*, PhD thesis, RWTH Aachen, 2014, CERN-THESIS-2013-301.
- [54] LHCb collaboration, R. Aaij *et al.*, *Precision luminosity measurements at LHCb*, JINST **9** (2014) P12005, arXiv:1410.0149.
- [55] T. Skwarnicki, *A study of the radiative cascade transitions between the Upsilon-prime and Upsilon resonances*, PhD thesis, Institute of Nuclear Physics, Krakow, 1986, DESY-F31-86-02.
- [56] D. Martínez Santos and F. Dupertuis, *Mass distributions marginalized over per-event errors*, Nucl. Instrum. Meth. **A764** (2014) 150, arXiv:1312.5000.
- [57] LHCb collaboration, R. Aaij *et al.*, *Measurement of the track reconstruction efficiency at LHCb*, JINST **10** (2015) P02007, arXiv:1408.1251.
- [58] M. Jacob and G. C. Wick, *On the general theory of collisions for particles with spin*, Annals Phys. **7** (1959) 404, [Annals Phys. **281** (2000) 774].

- [59] M. Pivk and F. R. Le Diberder, *sPlot: A statistical tool to unfold data distributions*, Nucl. Instrum. Meth. **A555** (2005) 356, [arXiv:physics/0402083](#).
- [60] ATLAS collaboration, G. Aad *et al.*, *Measurement of the differential non-prompt J/ψ production fraction in $\sqrt{s} = 13$ TeV pp collisions at the ATLAS experiment*, ATLAS-CONF-2015-030.
- [61] Particle Data Group, J. Beringer *et al.*, *Review of particle physics*, Phys. Rev. **D86** (2012) 010001.
- [62] M. Cacciari, M. L. Mangano, and P. Nason, *Gluon PDF constraints from the ratio of forward heavy quark production at the LHC at $\sqrt{s} = 7$ and 13 TeV*, [arXiv:1507.06197](#).
- [63] H.-S. Shao *et al.*, *Yields and polarizations of prompt J/ψ and $\psi(2S)$ production in hadronic collisions*, JHEP **05** (2015) 103, [arXiv:1411.3300](#).

Appendix

Change of efficiency with respect to polarization

The detection efficiency is affected by the polarisation, especially by the polarisation parameter λ_θ . Zero polarisation is assumed in these simulations since there is no prior knowledge of the polarisation of J/ψ mesons in pp collisions at 13 TeV, and only small polarisations have been found in all LHC quarkonia polarisation analyses [28–30, 36]. In Table 11, the increase of the total efficiency is given in bins of (p_T, y) of the J/ψ meson for a polarisation of $\lambda_\theta = -20\%$, compared to zero polarisation. This information facilitates the extrapolation of the cross-sections measured assuming zero polarisation to other polarisation values. The relative change in efficiency is linear, to 5% accuracy, between polarisation values of zero and 20%.

Table 11: The relative increase of the total efficiency (in %), for a -20% polarisation rather than zero, in different bins of p_T and y .

p_T [GeV/ c]	$2.0 < y < 2.5$	$2.5 < y < 3.0$	$3.0 < y < 3.5$	$3.5 < y < 4.0$	$4.0 < y < 4.5$
0 – 1	6.24 ± 0.35	4.89 ± 0.10	3.45 ± 0.11	3.31 ± 0.09	4.66 ± 0.17
1 – 2	5.58 ± 0.18	4.30 ± 0.07	2.94 ± 0.06	2.55 ± 0.03	2.82 ± 0.12
2 – 3	4.88 ± 0.14	3.47 ± 0.06	1.97 ± 0.04	1.52 ± 0.06	1.65 ± 0.13
3 – 4	4.77 ± 0.14	3.39 ± 0.06	1.94 ± 0.04	1.17 ± 0.07	1.13 ± 0.15
4 – 5	4.68 ± 0.14	3.34 ± 0.08	1.97 ± 0.04	1.20 ± 0.07	0.73 ± 0.14
5 – 6	4.43 ± 0.12	3.28 ± 0.10	2.03 ± 0.06	1.42 ± 0.06	0.75 ± 0.14
6 – 7	4.21 ± 0.09	3.03 ± 0.12	2.05 ± 0.08	1.57 ± 0.04	0.77 ± 0.14
7 – 8	3.88 ± 0.04	2.81 ± 0.15	1.98 ± 0.10	1.69 ± 0.05	0.74 ± 0.14
8 – 9	3.59 ± 0.15	2.65 ± 0.20	1.81 ± 0.11	1.65 ± 0.11	1.01 ± 0.13
9 – 10	3.53 ± 0.18	2.44 ± 0.24	1.81 ± 0.15	1.68 ± 0.16	1.17 ± 0.14
10 – 11	3.39 ± 0.27	2.30 ± 0.26	1.88 ± 0.22	1.73 ± 0.26	1.26 ± 0.14
11 – 12	3.09 ± 0.32	2.18 ± 0.38	1.47 ± 0.18	1.65 ± 0.27	1.35 ± 0.43
12 – 13	3.25 ± 0.45	1.65 ± 0.32	1.93 ± 0.36	1.49 ± 0.26	1.48 ± 0.21
13 – 14	2.72 ± 0.58	1.68 ± 0.32	1.71 ± 0.38	1.17 ± 0.27	1.36 ± 0.51

LHCb collaboration

R. Aaij³⁸, B. Adeva³⁷, M. Adinolfi⁴⁶, A. Affolder⁵², Z. Ajaltouni⁵, S. Akar⁶, J. Albrecht⁹, F. Alessio³⁸, M. Alexander⁵¹, S. Ali⁴¹, G. Alkhazov³⁰, P. Alvarez Cartelle⁵³, A.A. Alves Jr⁵⁷, S. Amato², S. Amerio²², Y. Amhis⁷, L. An³, L. Anderlini¹⁷, J. Anderson⁴⁰, G. Andreassi³⁹, M. Andreotti^{16,f}, J.E. Andrews⁵⁸, R.B. Appleby⁵⁴, O. Aquines Gutierrez¹⁰, F. Archilli³⁸, P. d'Argent¹¹, A. Artamonov³⁵, M. Artuso⁵⁹, E. Aslanides⁶, G. Auriemma^{25,m}, M. Baalouch⁵, S. Bachmann¹¹, J.J. Back⁴⁸, A. Badalov³⁶, C. Baesso⁶⁰, W. Baldini^{16,38}, R.J. Barlow⁵⁴, C. Barschel³⁸, S. Barsuk⁷, W. Barter³⁸, V. Batozskaya²⁸, V. Battista³⁹, A. Bay³⁹, L. Beaucourt⁴, J. Beddow⁵¹, F. Bedeschi²³, I. Bediaga¹, L.J. Bel⁴¹, V. Bellec³⁹, N. Belloli^{20,j}, I. Belyaev³¹, E. Ben-Haim⁸, G. Bencivenni¹⁸, S. Benson³⁸, J. Benton⁴⁶, A. Berezhnoy³², R. Bernet⁴⁰, A. Bertolin²², M.-O. Bettler³⁸, M. van Beuzekom⁴¹, A. Bien¹¹, S. Bifani⁴⁵, P. Billoir⁸, T. Bird⁵⁴, A. Birnkraut⁹, A. Bizzeti^{17,h}, T. Blake⁴⁸, F. Blanc³⁹, J. Blouw¹⁰, S. Blusk⁵⁹, V. Bocci²⁵, A. Bondar³⁴, N. Bondar^{30,38}, W. Bonivento¹⁵, S. Borghi⁵⁴, M. Borsato⁷, T.J.V. Bowcock⁵², E. Bowen⁴⁰, C. Bozzi¹⁶, S. Braun¹¹, M. Britsch¹⁰, T. Britton⁵⁹, J. Brodzicka⁵⁴, N.H. Brook⁴⁶, E. Buchanan⁴⁶, A. Bursche⁴⁰, J. Buytaert³⁸, S. Cadeddu¹⁵, R. Calabrese^{16,f}, M. Calvi^{20,j}, M. Calvo Gomez^{36,o}, P. Campana¹⁸, D. Campora Perez³⁸, L. Capriotti⁵⁴, A. Carbone^{14,d}, G. Carboni^{24,k}, R. Cardinale^{19,i}, A. Cardini¹⁵, P. Carniti^{20,j}, L. Carson⁵⁰, K. Carvalho Akiba^{2,38}, G. Casse⁵², L. Cassina^{20,j}, L. Castillo Garcia³⁸, M. Cattaneo³⁸, Ch. Cauet⁹, G. Cavallero¹⁹, R. Cenci^{23,s}, M. Charles⁸, Ph. Charpentier³⁸, M. Chefdeville⁴, S. Chen⁵⁴, S.-F. Cheung⁵⁵, N. Chiapolini⁴⁰, M. Chrzaszcz⁴⁰, X. Cid Vidal³⁸, G. Ciezarek⁴¹, P.E.L. Clarke⁵⁰, M. Clemencic³⁸, H.V. Cliff⁴⁷, J. Closier³⁸, V. Coco³⁸, J. Cogan⁶, E. Cogneras⁵, V. Cogoni^{15,e}, L. Cojocariu²⁹, G. Collazuol²², P. Collins³⁸, A. Comerma-Montells¹¹, A. Contu¹⁵, A. Cook⁴⁶, M. Coombes⁴⁶, S. Coquereau⁸, G. Corti³⁸, M. Corvo^{16,f}, B. Couturier³⁸, G.A. Cowan⁵⁰, D.C. Craik⁴⁸, A. Crocombe⁴⁸, M. Cruz Torres⁶⁰, S. Cunliffe⁵³, R. Currie⁵³, C. D'Ambrosio³⁸, E. Dall'Occo⁴¹, J. Dalseno⁴⁶, P.N.Y. David⁴¹, A. Davis⁵⁷, K. De Bruyn⁶, S. De Capua⁵⁴, M. De Cian¹¹, J.M. De Miranda¹, L. De Paula², P. De Simone¹⁸, C.-T. Dean⁵¹, D. Decamp⁴, M. Deckenhoff⁹, L. Del Buono⁸, N. Déléage⁴, M. Demmer⁹, D. Derkach⁶⁵, O. Deschamps⁵, F. Dettori³⁸, B. Dey²¹, A. Di Canto³⁸, F. Di Ruscio²⁴, H. Dijkstra³⁸, S. Donleavy⁵², F. Dordei¹¹, M. Dorigo³⁹, A. Dosil Suárez³⁷, D. Dossett⁴⁸, A. Dovbnya⁴³, K. Dreimanis⁵², L. Dufour⁴¹, G. Dujany⁵⁴, F. Dupertuis³⁹, P. Durante³⁸, R. Dzhelyadin³⁵, A. Dziurda²⁶, A. Dzyuba³⁰, S. Easo^{49,38}, U. Egede⁵³, V. Egorychev³¹, S. Eidelman³⁴, S. Eisenhardt⁵⁰, U. Eitschberger⁹, R. Ekelhof⁹, L. Eklund⁵¹, I. El Rifai⁵, Ch. Elsasser⁴⁰, S. Ely⁵⁹, S. Esen¹¹, H.M. Evans⁴⁷, T. Evans⁵⁵, A. Falabella¹⁴, C. Färber³⁸, N. Farley⁴⁵, S. Farry⁵², R. Fay⁵², D. Ferguson⁵⁰, V. Fernandez Albor³⁷, F. Ferrari¹⁴, F. Ferreira Rodrigues¹, M. Ferro-Luzzi³⁸, S. Filippov³³, M. Fiore^{16,38,f}, M. Fiorini^{16,f}, M. Firlej²⁷, C. Fitzpatrick³⁹, T. Fiutowski²⁷, K. Fohl³⁸, P. Fol⁵³, M. Fontana¹⁵, F. Fontanelli^{19,i}, R. Forty³⁸, O. Francisco², M. Frank³⁸, C. Frei³⁸, M. Frosini¹⁷, J. Fu²¹, E. Furfaro^{24,k}, A. Gallas Torreira³⁷, D. Galli^{14,d}, S. Gallorini²², S. Gambetta⁵⁰, M. Gandelman², P. Gandini⁵⁵, Y. Gao³, J. García Pardiñas³⁷, J. Garra Tico⁴⁷, L. Garrido³⁶, D. Gascon³⁶, C. Gaspar³⁸, R. Gauld⁵⁵, L. Gavardi⁹, G. Gazzoni⁵, D. Gerick¹¹, E. Gersabeck¹¹, M. Gersabeck⁵⁴, T. Gershon⁴⁸, Ph. Ghez⁴, S. Gianì³⁹, V. Gibson⁴⁷, O.G. Girard³⁹, L. Giubega²⁹, V.V. Gligorov³⁸, C. Göbel⁶⁰, D. Golubkov³¹, A. Golutvin^{53,38}, A. Gomes^{1,a}, C. Gotti^{20,j}, M. Grabalosa Gándara⁵, R. Graciani Diaz³⁶, L.A. Granado Cardoso³⁸, E. Graugés³⁶, E. Graverini⁴⁰, G. Graziani¹⁷, A. Grecu²⁹, E. Greening⁵⁵, S. Gregson⁴⁷, P. Griffith⁴⁵, L. Grillo¹¹, O. Grünberg⁶³, B. Gui⁵⁹, E. Gushchin³³, Yu. Guz^{35,38}, T. Gys³⁸, T. Hadavizadeh⁵⁵, C. Hadjivasiliou⁵⁹, G. Haefeli³⁹, C. Haen³⁸, S.C. Haines⁴⁷, S. Hall⁵³, B. Hamilton⁵⁸, X. Han¹¹,

S. Hansmann-Menzemer¹¹, N. Harnew⁵⁵, S.T. Harnew⁴⁶, J. Harrison⁵⁴, J. He³⁸, T. Head³⁹,
 V. Heijne⁴¹, K. Hennessy⁵², P. Henrard⁵, L. Henry⁸, E. van Herwijnen³⁸, M. Heß⁶³, A. Hicheur²,
 D. Hill⁵⁵, M. Hoballah⁵, C. Hombach⁵⁴, W. Hulsbergen⁴¹, T. Humair⁵³, N. Hussain⁵⁵,
 D. Hutchcroft⁵², D. Hynds⁵¹, M. Idzik²⁷, P. Ilten⁵⁶, R. Jacobsson³⁸, A. Jaeger¹¹, J. Jalocha⁵⁵,
 E. Jans⁴¹, A. Jawahery⁵⁸, F. Jing³, M. John⁵⁵, D. Johnson³⁸, C.R. Jones⁴⁷, C. Joram³⁸,
 B. Jost³⁸, N. Jurik⁵⁹, S. Kandybei⁴³, W. Kanso⁶, M. Karacson³⁸, T.M. Karbach^{38,†},
 S. Karodia⁵¹, M. Kecke¹¹, M. Kelsey⁵⁹, I.R. Kenyon⁴⁵, M. Kenzie³⁸, T. Ketel⁴², E. Khairullin⁶⁵,
 B. Khanji^{20,38,j}, C. Khurewathanakul³⁹, S. Klaver⁵⁴, K. Klimaszewski²⁸, O. Kochebina⁷,
 M. Kolpin¹¹, I. Komarov³⁹, R.F. Koopman⁴², P. Koppenburg^{41,38}, M. Kozeiha⁵, L. Kravchuk³³,
 K. Kreplin¹¹, M. Kreps⁴⁸, G. Krocker¹¹, P. Krokovny³⁴, F. Kruse⁹, W. Krzemien²⁸,
 W. Kucewicz^{26,n}, M. Kucharczyk²⁶, V. Kudryavtsev³⁴, A. K. Kuonen³⁹, K. Kurek²⁸,
 T. Kvaratskheliya³¹, D. Lacarrere³⁸, G. Lafferty⁵⁴, A. Lai¹⁵, D. Lambert⁵⁰, G. Lanfranchi¹⁸,
 C. Langenbruch⁴⁸, B. Langhans³⁸, T. Latham⁴⁸, C. Lazzeroni⁴⁵, R. Le Gac⁶, J. van Leerdam⁴¹,
 J.-P. Lees⁴, R. Lefèvre⁵, A. Leflat^{32,38}, J. Lefrançois⁷, E. Lemos Cid³⁷, O. Leroy⁶, T. Lesiak²⁶,
 B. Leverington¹¹, Y. Li⁷, T. Likhomanenko^{65,64}, M. Liles⁵², R. Lindner³⁸, C. Linn³⁸,
 F. Lionetto⁴⁰, B. Liu¹⁵, X. Liu³, D. Loh⁴⁸, I. Longstaff⁵¹, J.H. Lopes², D. Lucchesi^{22,q},
 M. Lucio Martinez³⁷, H. Luo⁵⁰, A. Lupato²², E. Luppi^{16,f}, O. Lupton⁵⁵, A. Lusiani²³,
 F. Machefert⁷, F. Maciuc²⁹, O. Maev³⁰, K. Maguire⁵⁴, S. Malde⁵⁵, A. Malinin⁶⁴, G. Manca⁷,
 G. Mancinelli⁶, P. Manning⁵⁹, A. Mapelli³⁸, J. Maratas⁵, J.F. Marchand⁴, U. Marconi¹⁴,
 C. Marin Benito³⁶, P. Marino^{23,38,s}, J. Marks¹¹, G. Martellotti²⁵, M. Martin⁶, M. Martinelli³⁹,
 D. Martinez Santos³⁷, F. Martinez Vidal⁶⁶, D. Martins Tostes², A. Massafferri¹, R. Matev³⁸,
 A. Mathad⁴⁸, Z. Mathe³⁸, C. Matteuzzi²⁰, A. Mauri⁴⁰, B. Maurin³⁹, A. Mazurov⁴⁵,
 M. McCann⁵³, J. McCarthy⁴⁵, A. McNab⁵⁴, R. McNulty¹², B. Meadows⁵⁷, F. Meier⁹,
 M. Meissner¹¹, D. Melnychuk²⁸, M. Merk⁴¹, E. Michielin²², D.A. Milanese⁶², M.-N. Minard⁴,
 D.S. Mitzel¹¹, J. Molina Rodriguez⁶⁰, I.A. Monroy⁶², S. Monteil⁵, M. Morandin²²,
 P. Morawski²⁷, A. Mordà⁶, M.J. Morello^{23,s}, J. Moron²⁷, A.B. Morris⁵⁰, R. Mountain⁵⁹,
 F. Muheim⁵⁰, D. Müller⁵⁴, J. Müller⁹, K. Müller⁴⁰, V. Müller⁹, M. Mussini¹⁴, B. Muster³⁹,
 P. Naik⁴⁶, T. Nakada³⁹, R. Nandakumar⁴⁹, A. Nandi⁵⁵, I. Nasteva², M. Needham⁵⁰, N. Neri²¹,
 S. Neubert¹¹, N. Neufeld³⁸, M. Neuner¹¹, A.D. Nguyen³⁹, T.D. Nguyen³⁹, C. Nguyen-Mau^{39,p},
 V. Niess⁵, R. Niet⁹, N. Nikitin³², T. Nikodem¹¹, A. Novoselov³⁵, D.P. O’Hanlon⁴⁸,
 A. Oblakowska-Mucha²⁷, V. Obraztsov³⁵, S. Ogilvy⁵¹, O. Okhrimenko⁴⁴, R. Oldeman^{15,e},
 C.J.G. Onderwater⁶⁷, B. Osorio Rodrigues¹, J.M. Otalora Goicochea², A. Otto³⁸, P. Owen⁵³,
 A. Oyanguren⁶⁶, A. Palano^{13,c}, F. Palombo^{21,t}, M. Palutan¹⁸, J. Panman³⁸, A. Papanestis⁴⁹,
 M. Pappagallo⁵¹, L.L. Pappalardo^{16,f}, C. Pappenheimer⁵⁷, W. Parker⁵⁸, C. Parkes⁵⁴,
 G. Passaleva¹⁷, G.D. Patel⁵², M. Patel⁵³, C. Patrignani^{19,i}, A. Pearce^{54,49}, A. Pellegrino⁴¹,
 G. Penso^{25,l}, M. Pepe Altarelli³⁸, S. Perazzini^{14,d}, P. Perret⁵, L. Pescatore⁴⁵, K. Petridis⁴⁶,
 A. Petrolini^{19,i}, M. Petruzzo²¹, E. Picatoste Olloqui³⁶, B. Pietrzyk⁴, T. Pilarš⁴⁸, D. Pinci²⁵,
 A. Pistone¹⁹, A. Piucci¹¹, S. Playfer⁵⁰, M. Plo Casasus³⁷, T. Poikela³⁸, F. Polci⁸,
 A. Poluektov^{48,34}, I. Polyakov³¹, E. Polycarpo², A. Popov³⁵, D. Popov^{10,38}, B. Popovici²⁹,
 C. Potterat², E. Price⁴⁶, J.D. Price⁵², J. Prisciandaro³⁷, A. Pritchard⁵², C. Prouve⁴⁶,
 V. Pugatch⁴⁴, A. Puig Navarro³⁹, G. Punzi^{23,r}, W. Qian⁴, R. Quagliani^{7,46}, B. Rachwal²⁶,
 J.H. Rademacker⁴⁶, M. Rama²³, M.S. Rangel², I. Raniuk⁴³, N. Rauschmayr³⁸, G. Raven⁴²,
 F. Redi⁵³, S. Reichert⁵⁴, M.M. Reid⁴⁸, A.C. dos Reis¹, S. Ricciardi⁴⁹, S. Richards⁴⁶, M. Rihl³⁸,
 K. Rinnert⁵², V. Rives Molina³⁶, P. Robbe^{7,38}, A.B. Rodrigues¹, E. Rodrigues⁵⁴,
 J.A. Rodriguez Lopez⁶², P. Rodriguez Perez⁵⁴, S. Roiser³⁸, V. Romanovsky³⁵,
 A. Romero Vidal³⁷, J. W. Ronayne¹², M. Rotondo²², J. Rouvinet³⁹, T. Ruf³⁸, P. Ruiz Valls⁶⁶,

J.J. Saborido Silva³⁷, N. Sagidova³⁰, P. Sail⁵¹, B. Saitta^{15,e}, V. Salustino Guimaraes²,
C. Sanchez Mayordomo⁶⁶, B. Sanmartin Sedes³⁷, R. Santacesaria²⁵, C. Santamarina Rios³⁷,
M. Santimaria¹⁸, E. Santovetti^{24,k}, A. Sarti^{18,l}, C. Satriano^{25,m}, A. Satta²⁴, D.M. Saunders⁴⁶,
D. Savrina^{31,32}, M. Schiller³⁸, H. Schindler³⁸, M. Schlupp⁹, M. Schmelling¹⁰, T. Schmelzer⁹,
B. Schmidt³⁸, O. Schneider³⁹, A. Schopper³⁸, M. Schubiger³⁹, M.-H. Schune⁷, R. Schwemmer³⁸,
B. Sciascia¹⁸, A. Sciubba^{25,l}, A. Semennikov³¹, N. Serra⁴⁰, J. Serrano⁶, L. Sestini²², P. Seyfert²⁰,
M. Shapkin³⁵, I. Shapoval^{16,43,f}, Y. Shcheglov³⁰, T. Shears⁵², L. Shekhtman³⁴, V. Shevchenko⁶⁴,
A. Shires⁹, B.G. Siddi¹⁶, R. Silva Coutinho^{48,40}, L. Silva de Oliveira², G. Simi²², M. Sirendi⁴⁷,
N. Skidmore⁴⁶, T. Skwarnicki⁵⁹, E. Smith^{55,49}, E. Smith⁵³, I.T. Smith⁵⁰, J. Smith⁴⁷, M. Smith⁵⁴,
H. Snoek⁴¹, M.D. Sokoloff^{57,38}, F.J.P. Soler⁵¹, F. Soomro³⁹, D. Souza⁴⁶, B. Souza De Paula²,
B. Spaan⁹, P. Spradlin⁵¹, S. Sridharan³⁸, F. Stagni³⁸, M. Stahl¹¹, S. Stahl³⁸, S. Stefkova⁵³,
O. Steinkamp⁴⁰, O. Stenyakin³⁵, S. Stevenson⁵⁵, S. Stoica²⁹, S. Stone⁵⁹, B. Storaci⁴⁰,
S. Stracka^{23,s}, M. Straticiuc²⁹, U. Straumann⁴⁰, L. Sun⁵⁷, W. Sutcliffe⁵³, K. Swientek²⁷,
S. Swientek⁹, V. Syropoulos⁴², M. Szczekowski²⁸, T. Szumlak²⁷, S. T'Jampens⁴, A. Tayduganov⁶,
T. Tekampe⁹, M. Teklishyn⁷, G. Tellarini^{16,f}, F. Teubert³⁸, C. Thomas⁵⁵, E. Thomas³⁸,
J. van Tilburg⁴¹, V. Tisserand⁴, M. Tobin³⁹, J. Todd⁵⁷, S. Tolk⁴², L. Tomassetti^{16,f}, D. Tonelli³⁸,
S. Topp-Joergensen⁵⁵, N. Tori⁵⁵, E. Tournefier⁴, S. Tourneur³⁹, K. Trabelsi³⁹, M.T. Tran³⁹,
M. Tresch⁴⁰, A. Trisovic³⁸, A. Tsaregorodtsev⁶, P. Tsopelas⁴¹, N. Tuning^{41,38}, A. Ukleja²⁸,
A. Ustyuzhanin^{65,64}, U. Uwer¹¹, C. Vacca^{15,e}, V. Vagnoni¹⁴, G. Valenti¹⁴, A. Vallier⁷,
R. Vazquez Gomez¹⁸, P. Vazquez Regueiro³⁷, C. Vázquez Sierra³⁷, S. Vecchi¹⁶, J.J. Velthuis⁴⁶,
M. Veltri^{17,g}, G. Veneziano³⁹, M. Vesterinen¹¹, B. Viaud⁷, D. Vieira², M. Vieites Diaz³⁷,
X. Vilasis-Cardona^{36,o}, V. Volkov³², A. Vollhardt⁴⁰, D. Volyanskyy¹⁰, D. Voong⁴⁶,
A. Vorobyev³⁰, V. Vorobyev³⁴, C. Voß⁶³, J.A. de Vries⁴¹, R. Waldi⁶³, C. Wallace⁴⁸, R. Wallace¹²,
J. Walsh²³, S. Wandernoth¹¹, J. Wang⁵⁹, D.R. Ward⁴⁷, N.K. Watson⁴⁵, D. Websdale⁵³,
A. Weiden⁴⁰, M. Whitehead⁴⁸, G. Wilkinson^{55,38}, M. Wilkinson⁵⁹, M. Williams³⁸,
M.P. Williams⁴⁵, M. Williams⁵⁶, T. Williams⁴⁵, F.F. Wilson⁴⁹, J. Wimberley⁵⁸, J. Wishahi⁹,
W. Wislicki²⁸, M. Witek²⁶, G. Wormser⁷, S.A. Wotton⁴⁷, S. Wright⁴⁷, K. Wyllie³⁸, Y. Xie⁶¹,
Z. Xu³⁹, Z. Yang³, J. Yu⁶¹, X. Yuan³⁴, O. Yushchenko³⁵, M. Zangoli¹⁴, M. Zavertyaev^{10,b},
L. Zhang³, Y. Zhang³, A. Zhelezov¹¹, A. Zhokhov³¹, L. Zhong³, S. Zucchelli¹⁴.

¹ Centro Brasileiro de Pesquisas Físicas (CBPF), Rio de Janeiro, Brazil

² Universidade Federal do Rio de Janeiro (UFRJ), Rio de Janeiro, Brazil

³ Center for High Energy Physics, Tsinghua University, Beijing, China

⁴ LAPP, Université Savoie Mont-Blanc, CNRS/IN2P3, Annecy-Le-Vieux, France

⁵ Clermont Université, Université Blaise Pascal, CNRS/IN2P3, LPC, Clermont-Ferrand, France

⁶ CPPM, Aix-Marseille Université, CNRS/IN2P3, Marseille, France

⁷ LAL, Université Paris-Sud, CNRS/IN2P3, Orsay, France

⁸ LPNHE, Université Pierre et Marie Curie, Université Paris Diderot, CNRS/IN2P3, Paris, France

⁹ Fakultät Physik, Technische Universität Dortmund, Dortmund, Germany

¹⁰ Max-Planck-Institut für Kernphysik (MPIK), Heidelberg, Germany

¹¹ Physikalisches Institut, Ruprecht-Karls-Universität Heidelberg, Heidelberg, Germany

¹² School of Physics, University College Dublin, Dublin, Ireland

¹³ Sezione INFN di Bari, Bari, Italy

¹⁴ Sezione INFN di Bologna, Bologna, Italy

¹⁵ Sezione INFN di Cagliari, Cagliari, Italy

¹⁶ Sezione INFN di Ferrara, Ferrara, Italy

¹⁷ Sezione INFN di Firenze, Firenze, Italy

¹⁸ Laboratori Nazionali dell'INFN di Frascati, Frascati, Italy

- ¹⁹ *Sezione INFN di Genova, Genova, Italy*
- ²⁰ *Sezione INFN di Milano Bicocca, Milano, Italy*
- ²¹ *Sezione INFN di Milano, Milano, Italy*
- ²² *Sezione INFN di Padova, Padova, Italy*
- ²³ *Sezione INFN di Pisa, Pisa, Italy*
- ²⁴ *Sezione INFN di Roma Tor Vergata, Roma, Italy*
- ²⁵ *Sezione INFN di Roma La Sapienza, Roma, Italy*
- ²⁶ *Henryk Niewodniczanski Institute of Nuclear Physics Polish Academy of Sciences, Kraków, Poland*
- ²⁷ *AGH - University of Science and Technology, Faculty of Physics and Applied Computer Science, Kraków, Poland*
- ²⁸ *National Center for Nuclear Research (NCBJ), Warsaw, Poland*
- ²⁹ *Horia Hulubei National Institute of Physics and Nuclear Engineering, Bucharest-Magurele, Romania*
- ³⁰ *Petersburg Nuclear Physics Institute (PNPI), Gatchina, Russia*
- ³¹ *Institute of Theoretical and Experimental Physics (ITEP), Moscow, Russia*
- ³² *Institute of Nuclear Physics, Moscow State University (SINP MSU), Moscow, Russia*
- ³³ *Institute for Nuclear Research of the Russian Academy of Sciences (INR RAN), Moscow, Russia*
- ³⁴ *Budker Institute of Nuclear Physics (SB RAS) and Novosibirsk State University, Novosibirsk, Russia*
- ³⁵ *Institute for High Energy Physics (IHEP), Protvino, Russia*
- ³⁶ *Universitat de Barcelona, Barcelona, Spain*
- ³⁷ *Universidad de Santiago de Compostela, Santiago de Compostela, Spain*
- ³⁸ *European Organization for Nuclear Research (CERN), Geneva, Switzerland*
- ³⁹ *Ecole Polytechnique Fédérale de Lausanne (EPFL), Lausanne, Switzerland*
- ⁴⁰ *Physik-Institut, Universität Zürich, Zürich, Switzerland*
- ⁴¹ *Nikhef National Institute for Subatomic Physics, Amsterdam, The Netherlands*
- ⁴² *Nikhef National Institute for Subatomic Physics and VU University Amsterdam, Amsterdam, The Netherlands*
- ⁴³ *NSC Kharkiv Institute of Physics and Technology (NSC KIPT), Kharkiv, Ukraine*
- ⁴⁴ *Institute for Nuclear Research of the National Academy of Sciences (KINR), Kyiv, Ukraine*
- ⁴⁵ *University of Birmingham, Birmingham, United Kingdom*
- ⁴⁶ *H.H. Wills Physics Laboratory, University of Bristol, Bristol, United Kingdom*
- ⁴⁷ *Cavendish Laboratory, University of Cambridge, Cambridge, United Kingdom*
- ⁴⁸ *Department of Physics, University of Warwick, Coventry, United Kingdom*
- ⁴⁹ *STFC Rutherford Appleton Laboratory, Didcot, United Kingdom*
- ⁵⁰ *School of Physics and Astronomy, University of Edinburgh, Edinburgh, United Kingdom*
- ⁵¹ *School of Physics and Astronomy, University of Glasgow, Glasgow, United Kingdom*
- ⁵² *Oliver Lodge Laboratory, University of Liverpool, Liverpool, United Kingdom*
- ⁵³ *Imperial College London, London, United Kingdom*
- ⁵⁴ *School of Physics and Astronomy, University of Manchester, Manchester, United Kingdom*
- ⁵⁵ *Department of Physics, University of Oxford, Oxford, United Kingdom*
- ⁵⁶ *Massachusetts Institute of Technology, Cambridge, MA, United States*
- ⁵⁷ *University of Cincinnati, Cincinnati, OH, United States*
- ⁵⁸ *University of Maryland, College Park, MD, United States*
- ⁵⁹ *Syracuse University, Syracuse, NY, United States*
- ⁶⁰ *Pontifícia Universidade Católica do Rio de Janeiro (PUC-Rio), Rio de Janeiro, Brazil, associated to ²*
- ⁶¹ *Institute of Particle Physics, Central China Normal University, Wuhan, Hubei, China, associated to ³*
- ⁶² *Departamento de Física, Universidad Nacional de Colombia, Bogota, Colombia, associated to ⁸*
- ⁶³ *Institut für Physik, Universität Rostock, Rostock, Germany, associated to ¹¹*
- ⁶⁴ *National Research Centre Kurchatov Institute, Moscow, Russia, associated to ³¹*
- ⁶⁵ *Yandex School of Data Analysis, Moscow, Russia, associated to ³¹*
- ⁶⁶ *Instituto de Física Corpuscular (IFIC), Universitat de Valencia-CSIC, Valencia, Spain, associated to ³⁶*
- ⁶⁷ *Van Swinderen Institute, University of Groningen, Groningen, The Netherlands, associated to ⁴¹*

- ^a *Universidade Federal do Triângulo Mineiro (UFMT), Uberaba-MG, Brazil*
- ^b *P.N. Lebedev Physical Institute, Russian Academy of Science (LPI RAS), Moscow, Russia*
- ^c *Università di Bari, Bari, Italy*
- ^d *Università di Bologna, Bologna, Italy*
- ^e *Università di Cagliari, Cagliari, Italy*
- ^f *Università di Ferrara, Ferrara, Italy*
- ^g *Università di Urbino, Urbino, Italy*
- ^h *Università di Modena e Reggio Emilia, Modena, Italy*
- ⁱ *Università di Genova, Genova, Italy*
- ^j *Università di Milano Bicocca, Milano, Italy*
- ^k *Università di Roma Tor Vergata, Roma, Italy*
- ^l *Università di Roma La Sapienza, Roma, Italy*
- ^m *Università della Basilicata, Potenza, Italy*
- ⁿ *AGH - University of Science and Technology, Faculty of Computer Science, Electronics and Telecommunications, Kraków, Poland*
- ^o *LIFAELS, La Salle, Universitat Ramon Llull, Barcelona, Spain*
- ^p *Hanoi University of Science, Hanoi, Viet Nam*
- ^q *Università di Padova, Padova, Italy*
- ^r *Università di Pisa, Pisa, Italy*
- ^s *Scuola Normale Superiore, Pisa, Italy*
- ^t *Università degli Studi di Milano, Milano, Italy*
- [†] *Deceased*